Construction and Building Materials 425 (2024) 136052

Contents lists available at ScienceDirect

Construction and Building Materials

journal homepage: www.elsevier.com/locate/conbuildmat

Piezoresistivity and piezopermittivity of cement-based sensors under quasi-static stress and changing moisture

Jiacheng Zhang [a,b,c,*,1], Andrew Heath [b,d,f,2], Richard J. Ball [b,c,e,*,3], Binling Chen [b,h,4], Linzhen Tan [b,i,5], Guisheng Li [a,*,6], Jingbang Pan [b,c,g,7], Tugce Busra Su-Cadirci [j,8], Kevin Paine [b,e,9]

[a] School of Materials and Chemistry, University of Shanghai for Science and Technology, Shanghai, 200093, PR China
[b] Department of Architecture and Civil Engineering, University of Bath, Claverton Down, Bath, BA2 7AY, United Kingdom
[c] Centre for Integrated Materials, Processes & Structures (IMPS), University of Bath, Claverton Down, Bath, BA2 7AY, United Kingdom
[d] Centre for Infrastructure, Geotechnical and Water Engineering Research (IGWE), University of Bath, Claverton Down, Bath, BA2 7AY, United Kingdom
[e] Centre for Climate Adaptation & Environment Research (CAER), University of Bath, Claverton Down, Bath, BA2 7AY, United Kingdom
[f] Institute for Advanced Automotive Propulsion Systems (IAAPS), University of Bath, Claverton Down, Bath, BA2 7AY, United Kingdom
[g] Centre for Digital, Manufacturing & Design (dMaDe), University of Bath, Claverton Down, Bath, BA2 7AY, United Kingdom
[h] School of Mechanical Engineering, Beijing Institute of Technology, Beijing, 100081, PR China
[i] Pavement Materials and Research, AECOM Limited, Nottingham, NG9 6RZ, United Kingdom
[j] Department of Architecture, Abdullah Gul University, Kayseri, 38080, Turkey

ARTICLE INFO

Keywords:
Carbon fibers
Self-sensing cement-based sensor
Electrochemical impedance spectroscopy
Piezoresistivity
Piezopermittivity
Moisture content

ABSTRACT

Integrated cement-based sensors offer an economic alternative to extrinsic sensors for health monitoring applications in concrete structures due to their high strength to cost ratio, geometrical versatility, low shrinkage, and natural compatibility. Nonetheless, their performance under in-service conditions were in lack of investigations. While the piezoresistivity (change in resistance with stress) has been commonly used for mechanical sensing, the piezopermittivity (change in capacitive reactance with stress) is rarely characterized. Exploiting the high relative permittivity and electrical conductivity of carbon fibre reinforced cement-based sensors, this study investigates the piezoresistivity and piezopermittivity under changing stress and moisture using electrochemical impedance spectroscopy (EIS). Two types of sensors were evaluated: one containing 0.5 vol% of carbon fibres whose electrical conductivity was ionically dominant, and another with electronically dominant (1.2 vol% of carbon fibres) conductivity. Results highlighted that the piezopermittivity is "moisture content-dominant" whilst the piezoresistivity is "fibre content-dominant". As the moisture content decreased, the sensitivity of piezopermittivity for both sensor types decreased, while the sensitivity of piezoresistivity decreased for the ionically dominant sensor but increased for the electronically dominant sensor. The piezoresistivity of the electronically dominant sensor was less sensitive than piezopermittivity at a water saturation of 80%. Conversely, the piezoresistivity of the ionically dominant sensor was more sensitive than piezopermittivity at the tested water saturations $\leq$ 80%. For the first time, this study presents the combined effects of moisture and fibre content on the pressure sensitive response of cement-based sensors through a dual-phase (i.e., piezoresistivity and piezopermittivity) EIS interpretation technique, providing valuable information to benefit further behaviour prediction and single-effect recognition in the field scenario where the sensors are subject to simultaneous

* Corresponding author.
E-mail addresses: J.Zhang@bath.ac.uk (J. Zhang), R.J.Ball@bath.ac.uk (R.J. Ball), liguisheng@usst.edu.cn (G. Li).
[1] https://orcid.org/0000-0001-5380-0050
[2] https://orcid.org/0000-0003-0154-0941
[3] https://orcid.org/0000-0002-7413-3944
[4] https://orcid.org/0000-0003-0719-7398
[5] https://orcid.org/0000-0002-4569-8399
[6] https://orcid.org/0000-0002-4522-8936
[7] https://orcid.org/0000-0001-6320-5685
[8] https://orcid.org/0000-0001-6617-0924
[9] https://orcid.org/0000-0001-7455-7002

https://doi.org/10.1016/j.conbuildmat.2024.136052
Received 26 November 2023; Received in revised form 18 March 2024; Accepted 27 March 2024
Available online 2 April 2024

environmental effects causing moisture variations such as temperature and humidity variations, freeze-thawing, and so on.

1. Introduction

Real-time, in-situ health monitoring of concrete structures enables timely and precise remediation of defective locations which mitigates the environmental impact of delayed repair (i.e., energy, material consumption), saves labour cost, and potentially prevents catastrophic collapse. Since the early 1990s, intrinsic self-sensing cement-based sensors have been extensively studied owing to their great potential as an alternative to extrinsic sensors for the health monitoring of concrete structures [1–13]. Intrinsic self-sensing cement-based sensors possess an electrically conductive network formed by the addition of conductive fillers into cement paste, mortar, or concrete, which not only reduces the discontinuities of the cementitious matrix thereby enhancing the electrical conductivity required for self-sensing, but also improves other physical properties such as the reduced drying shrinkage and enhanced mechanical performance [14–24]. These improvements in behaviour, in combination with the advantage of natural compatibility with concrete structures, allows for multi-purpose health monitoring of concrete structures in terms of strain/stress, cracking/damage, temperature, crack healing, and so on [25–31], which render cement-based sensors preferable over extrinsic sensors for many applications [32–34].

Cement-based sensors can be integrated with electrical measurement techniques to form a structural health monitoring system. Conventional measurement technique is to use DC signal. Although it is cheap and easy to perform, an accompanying monotonic polarization effect would occur which enhances with the increasing moisture content and with the increasing excitation time, in turn increasing the signal noise and even blocking the signal output [20,35–37]. Electrochemical impedance spectroscopy (EIS), known for its rapid and non-destructive material analysis capabilities, has been a reliable tool for the characterization of cementitious materials in terms of early hydration, carbonation, dewatering, corrosion, permeability/durability, microstructural analysis, loading, cracking, crack healing, and etc. [23,34,38–57]. By the AC signal excitation and the “spectroscopy” over a wide frequency range from mHz to MHz, EIS can differentiate the conduction and dielectric mechanisms operative in an inhomogeneous composite like hardened cement. Whilst presenting multi-parameter characterization (e.g., resistance, reactance, phase angle, etc.), EIS exhibits a distinct advantage over DC methods as the signal interference from the polarization effect is minimized.

Despite extensive research under laboratory conditions on the microstructure, stationary electrical behaviour, mechanical behaviour, dispersion of functional fillers, and stress/strain sensing behaviour, the effective use of cement-based sensors has been limited because their in-situ behaviour is rarely known. Few researchers have explored the stress/strain self-sensing behaviour under varying environmental conditions. The surrounding environment can influence the stress/strain self-sensing behaviour of cement-based sensors via various actions such as thermal expansion/shrinkage, freeze-thaw, mobilisation of salts, chloride ingress, sulphate attack, and so on. However, the most fundamental and primary action to understand is a change in moisture content. Because the moisture, as one of the most important components in a hardened cementitious material, contributes to the ionic conduction through cementitious matrix, which can influence the stress/strain self-sensing signal response of cement-based sensors. More importantly, evaluating the influence of moisture content on the stress/strain self-sensing performance indirectly evaluates the influence of ambient humidity.

Studies on the moisture dependence of the stress/strain self-sensing behaviour of cement-based sensors are limited, and these can be categorized into three types based on the conductive fillers used: macro-scale fillers alone [19,58–61], hybrid fillers [20,62–65], and nano-scale fillers alone [37,66,67]. An investigation on the moisture dependence of piezoresistivity for a cement-based sensor incorporating nano-scale carbon black was conducted by Dong et al. [37] with detailed increments of moisture content from dried state to full water saturation, where the sensing sensitivity firstly increased to peak at a moisture content of 8% before decreasing. They attributed this behaviour to the mechanism that the moisture can encapsulate the carbon black particles at higher moisture contents due to their nano-scale dimension, blocking the electronic conduction between the adjacent carbon black particles. A similar behaviour of piezoresistivity over increasing moisture content was also found using carbon nanotubes in a cement-based sensor [66]. This behaviour was attributed to the enhanced ionic conduction and field emission on the tips of the carbon nanotubes with the increasing moisture, and the stabilization of conductive channels at full water saturation exhibiting minimal changes with stress. For cement-based sensors incorporating hybrid fillers, Han et al. [66] reported a monotonic decreasing sensing sensitivity when drying from 0 to 7 days with carbon fibres and carbon black. Similar results on the moisture dependence of sensing sensitivity was reported by Zhang et al. [63] where hybrid fillers (carbon nanotube and carbon black) were used. While employing macro-scale fillers, Wen and Chung [59] reported that the strain sensing sensitivity of carbon fibre reinforced cement-based sensors was lower in the wet state compared to that in a relatively drier state. They proposed that the effective opening size of the microcrack was reduced while the sensor was in the wet state hence a reduced sensitivity. In contrast, Maier [64] found an acceptable piezoresistivity in the saturated state for a cement-based sensor with steel fibres, but explicitly no piezoresistive response in the dried state. Baeza et al. [19] discovered an optimal saturation degree of 46% where the highest sensing sensitivity was detected on a carbon fibre reinforced cement-based sensor, whilst a higher optimal saturation degree of 71% was reported in their later study using hybrid fillers (i.e., carbon nanotube and graphite) [65]. Apart from the moisture dependence of stress/strain sensing sensitivity, both Hong et al. [20] and Dong et al. [37] reported increased signal noise with the increasing water content, which was attributed to the pronounced DC polarization effect at higher water contents hindering the signal output.

All the above studies have employed the conventional technique of resistance-based measurement, where the ionic conduction changes with the changing moisture content hence the change in the piezoresistivity of the material. The moisture content not only dominates the ionic conduction through the connected pores [44,68,69], meanwhile also being an important contributor to the capacitive properties (i.e., capacitive reactance, capacitance, and relative permittivity) of cementitious materials [42]. Also, due to the increased solid-liquid interfaces by the inclusion of conductive fillers, the effective (or volumetric) relative permittivity of a hardened cement-based sensor (i.e., with a curing age above 28 days) is usually higher than a plain mix, presenting values from 20 to 2500 [16,70–72] depending on the filler content, mix design, etc., which is also much higher than that of common dielectrics for the production of commercial stress sensitive sensors [73–76]. Higher relative permittivity ensures greater changes in capacitive property under stress/strain which renders cement-based sensors a promising capacitive stress sensor. Therefore, it is also important to understand the influence of moisture content on the capacitive stress sensing behaviour of cement-based sensors. The stress sensitive behaviour provided by the capacitive properties of the material is termed as piezopermittivity [77].

Research on the piezopermittivity of cement-based sensor are scarce and still awaits attention. The piezopermittivity of cement-based sensor

can be characterized by measuring the changes in capacitive reactance, capacitance, or relative permittivity as the stress/strain changes. Fu et al. [78] reported that under self-sensing of monotonic compression, both the capacitive reactance and resistance of carbon fibre reinforced cement-based sensor increased with the increasing strain at a strain range of 0 – 0.00175, where the increase in capacitive reactance was always larger than that of resistance. Wen and Chung [16] reported that under self-sensing of cyclic compression, the relative permittivity of cement-based sensor was positively correlated to the stress at a stress range of 0 – 6.4 MPa. In the later studies of Chung's research team [21, 79–82], piezopermittivity was characterized on asphalt and cementitious materials without the inclusion of conductive fillers where the capacitance increased with the increasing compressive stress, proposing that self-sensing of stress/strain based on piezopermittivity is advantageous over piezoresistivity due to higher sensitivity, easier electrode configuration, and being application friendly to existing structures without the need for conductive fillers (or the need for extrinsic sensors). However, Hou et al. [83] suggests that AC resistance-based measurement is preferable than capacitance-based measurement because of the higher gauge factor of resistance-based measurement on UHPC incorporating steel fibres reported in their study.

In the literature, studies showed limitations in terms of the measurement technique and material configurations. The DC resistance-based measurement in some studies lead to increased signal noise once the moisture content was elevated hence hindering the signal processing [20,37]. In some studies, the AC measurement technique, either in terms of piezoresistivity or piezopermittivity, was configured at a lower frequency which was not the operative frequency of the bulk mechanism [78,83]. Most of the studies employed limited filler content, leading to the limited understanding on how the filler and moisture contents depend on each other hence the complex behaviour of piezoresistivity and piezopermittivity [37,60,61]. Therefore, this work aims to address the above issues by determining the piezoresistivity and piezopermittivity of cement-based sensors incorporating macro-scale chopped carbon fibres under various moisture contents and fibre loadings.

In this study, The stress self-sensing work was undertaken on cement-based sensors determined in the previous work [72] as having three characteristic fibre loadings: a plain mortar without carbon fibres whose conduction of electricity was totally ionic (with a conductivity of 0.013 S/m and a relative permittivity of 313 and at frequencies 1 MHz – 10 MHz and in water saturated state), a cement-based sensor with 0.5 vol% of carbon fibres which was also ionically dominant (with a conductivity of 0.05 S/m and a relative permittivity of 473 at frequencies 1 MHz – 10 MHz and in water saturated state), and a cement-based sensor with 1.2 vol% of carbon fibres which was electronically dominant (with a conductivity of 0.2 S/m and a relative permittivity of 591 at frequencies 1 MHz – 10 MHz and in water saturated state). The sensors were tested for stress self-sensing behaviour under two specified moisture scenarios: one is the random water saturation degree where the internal moisture of the sensors was passively exchanged with the outside environment for three days. This scenario is likely to happen in most in-situ conditions. Another is the designated water saturation degrees where the internal moisture was controlled by drying a fully water saturated sensor monotonically to 80%, 50%, and 30%. This scenario is aimed to have an in-depth investigation on the underlying mechanism of how the fibre and moisture contents influence collectively on the pressure sensitive properties of cement-based sensors at fully controlled water saturation degrees. Mercury intrusion porosimetry (MIP) and polarized light microscopy were used for the determination of the microstructure of cement-based sensors. EIS was used for the measurement of electrical signal response of cement-based sensors, where the piezoresistivity was characterized by resistance and the piezopermittivity was characterized by capacitive reactance. The bulk response of the measured complex impedance was used to extract the resistance and the capacitive reactance which situated at frequencies from1 kHz to 10 MHz. The sensing recoverability, sensing repeatability, sensing linearity, sensing sensitivity, and sensing stability were all quantified.

For the first time, this study presents the difference in behaviour of piezoresistivity and piezopermittivity of carbon fibre reinforced cement-based sensors under the combined effects of moisture and fibre contents. The results and mechanisms revealed in this study enables a more versatile measurement methodology for electrical signal response and a more strategic approach for the control of fibre contents under various in-service conditions. Also, this study has proved that cement-based sensors can be properly used in the absence of complex chemical modifications and extrinsic sensors for the compensation of environmental effects. The data in this study can benefit the further in-situ case studies under complex environmental conditions and the confidence of this technology for mass scale application.

2. Experimental programme

2.1. Materials and fabrication

Raw materials for the preparation of the mortar matrix were deionized water, CEMI42.5 R cement conforming to BS EN 197–1 and standard testing sand conforming to BS EN 196–1. The mixing ratio of water: cement: sand was fixed at 0.45: 1: 3 for all mortar matrices. Polyacrylonitrile (PAN-based) chopped carbon fibres (SGL Carbon Fibers Ltd, Wiesbaden, Germany) were used as conductive fillers for their high electrical conductivity and strength-to-cost ratio (Table 1). Cement-based sensors were made by dispersing carbon fibres into the mortar matrix at contents of 0.5% and 1.2% of total volume. Polycarboxylate superplasticizer (PERAMIN® COMPAC, Upplands Vasby, Sweden), known for its "double dispersion" mechanism of making the surfaces of both the cement grain and carbon fibres hydrophilic [84–87], was employed with a dosage of 0.4% by mass of cement to assist in the dispersion of the fibres and improve the workability of the mix. Tributyl phosphate (SIGMA-ALDRICH, Dorset, UK) was used as defoamer to reduce air bubbles and the dosage was 6 drops for each mix (0.5 mL per drop from a PE pipette), as determined experimentally to be the lowest content which resulted in minimal bubble formation.

Fabrication of cement-based sensors followed the concept that the surface of the fibres should be made hydrophilic by the polycarboxylate superplasticizer prior to being mixed with cement and sand for the assistance of fibre dispersion in the wet mix [88,89]. Initially, a fibrous solution was made by mixing the carbon fibres with the whole portion of the mixing water and polycarboxylate superplasticizer in a glass beaker. The glass beaker containing the fibrous solution was then put in an ultrasonicator (Allendale Ultrasonics, Hoddesdon, UK) at a frequency and temperature of 40 kHz and 45°C, respectively. Meanwhile the defoamer was slowly dropped into the fibrous solution and manual stirring was also performed gently using a glass stirrer. After 30 minutes of ultrasonic vibration, the fibrous solution was mixed with the whole portion of cement in an electronic blender (CONTROLS LTD, Hertfordshire, UK) for 5 minutes. Then, the whole portion of the sand was added into the mixture, which was blended for another 5 minutes.

The mixture was placed into a stainless-steel mould conforming to BS EN 196–1, where three samples each with standard dimension 40 × 40 × 160 mm were cast at one time (Fig. 1a). Then, the mould was fixed on a vibration platform and vibrated for the compaction and reduction of the air bubbles in the mixture. After compaction, four stainless-steel rod electrodes with a dimension of 3 mm of diameter and 50 mm of length were inserted into the mixture to a depth of 30 mm (Fig. 1b). The purpose of the embedment of the electrodes is to ensure an intimate contact between the electrodes and the sensor matrix. Also, the rod-shaped electrodes can minimize the contact area between the electrodes and the sensor matrix. Therefore, such electrode configuration can reduce the susceptibility for the formation of weak planes under stress, hence contributing to a stable signal transmission for the evaluation of

Table 1
Technical specifications of chopped carbon fibres.

Density (g/cm^3)	Fibre length (mm)	Filament diameter (μm)	Tensile Strength (GPa)	Tensile Modulus (GPa)	Elongation at break (%)	Electrical resistivity (ohm• m)
1.8	6	7.5	4	240	1.7	1.5×10^{-5}

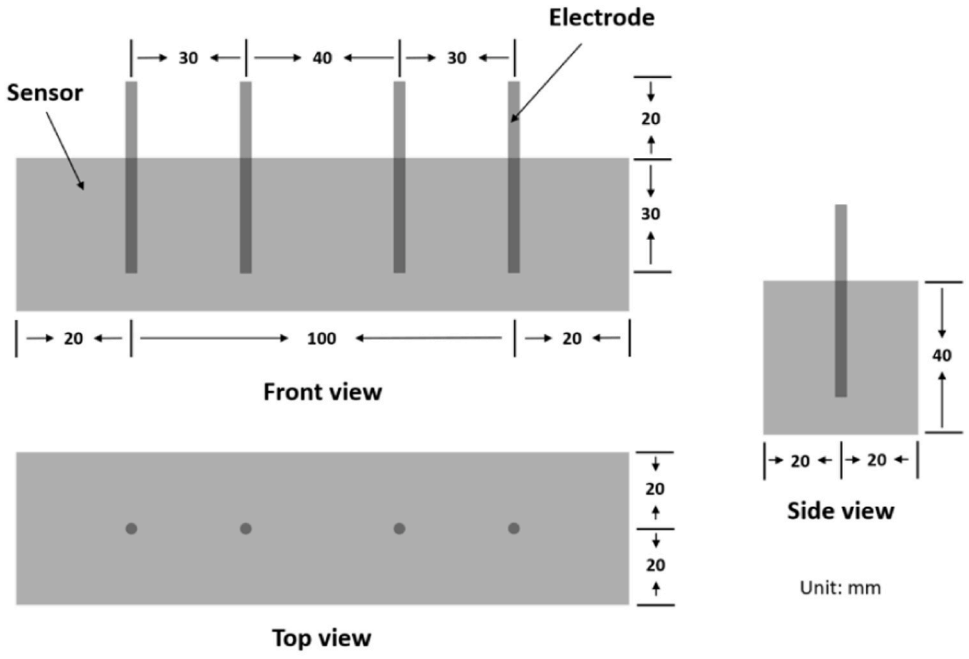

(a)

(b)

Fig. 1. Fabrication of samples: (a) electrode configuration and dimension of prismatic samples at front, top, and side views, unit in mm (b) fresh sample in the mould sealed with PVC film.

volumetric impedance. Finally, the mould containing the mixture was wrapped with PVC film to minimize the influence of drying and carbonation, and placed in the laboratory condition (20 ± 5°C, 50% RH). After 24 hours, samples were demoulded and submerged under water at 21°C for curing. The samples were taken out for experiments at a curing age of 97 days. At this curing age the ionic conductivity of the pore fluid can be considered to be stabilized [90]. For the ease of expression, the testing samples were denoted based on their composition: the mortar matrix without carbon fibre was referred to as PM (as in plain mortar), and the mortar matrix incorporating 0.5 and 1.2 vol% of carbon fibres, which were the cement-based sensors, were referred to as S0.5 and S1.2, respectively.

2.2. Methods

2.2.1. Drying process

2.2.1.1. Preliminary drying. Considering the large size of the samples, an environmental chamber was employed for drying the samples to designated saturation degrees. A preliminary drying procedure was conducted to understand the relationship between the saturation degree and the cumulative drying time for both the plain mortar and the sensors. A group of reference samples were removed from the water tank at the curing age of 97 days and constantly dried in the environmental chamber from full water-saturation to defined mass equilibrium condition under 60°C and 5% RH, during which the mass of each sample and the duration of the drying were recorded at specified time intervals. This method ensured an accurate determination of saturation degree without hysteretic effects influencing results. The mass equilibrium in this study was defined as less than 0.01 g of change in the mass for three consecutive mass weighing at a time interval of 120 hours. The reference samples had the same mix design, fabrication method and environment, curing condition, and curing age as the samples for self-sensing tests. Therefore, it was assumed that they share a similar pore structure and moisture content [37]. The moisture content (MC) was initially obtained through:

$$MC = \frac{M_t - M_e}{M_e - M_s} \times 100\% \quad (1)$$

where M_t was the mass (unit in g) of the samples at a certain drying time, M_e the mass at the condition of mass equilibrium as defined above, and M_s the mass of the stainless-steel electrodes.

The saturation degree (SD) was therefore calculated by:

$$SD = \frac{MC_t}{MC_0} \times 100\% \quad (2)$$

where MC_t the moisture content at a certain drying time, MC_0 the moisture content at zero drying time (full saturation).

The cumulative drying time to reach designated saturation degrees of 80%, 50%, and 30% for each reference sample was recorded in Fig. 2a and the time to reach mass equilibrium was recorded in Fig. 2b. Although drying at 60°C is lower than some earlier studies [91–93], it is inevitable that elevated temperatures can negatively affect the sample microstructures, further affecting the self-sensing behaviour. This was evaluated in conjunction with mercury intrusion porosimetry (MIP).

2.2.1.2. Drying for self-sensing

2.2.1.2.1. Designated saturation degrees. Based on the above preliminary knowledge of the relationship between water saturation degree and drying time, monotonic drying for self-sensing was conducted. Likewise, the samples were removed from the water tank at the curing age of 97 days and the drying was immediately initiated at a fully water-saturated condition under the same environment as the reference samples. The drying was stopped at the timestamps recorded in Fig. 2a, which signified that a designated saturation degree had been reached. Then, sample was sealed in a zip-lock bag and placed in a sealed plastic container to minimize the moisture exchange with the environment and naturally cooled in the laboratory (20 ± 5°C, 50% RH) for at least 24 hours until its temperature reached equilibrium to ambient environment and its internal moisture distribution reached equilibrium. Self-sensing tests at designated degrees of saturation were performed thereafter.

2.2.1.2.2. Randomized saturation degrees. A group of water saturated samples, which also had a curing age of 97 days and were from the same mixing batch as those under drying, were placed on an elevated stainless-steel rack and exposed to the outside environment for 3 days. This allowed for random moisture exchanges between the environment and the samples from day to night. Then, samples were collected back to the laboratory and also sealed in the zip-lock bag for at least 24 hours. Self-sensing tests at randomized saturation degrees were performed thereafter.

2.2.2. Self-sensing configurations

2.2.2.1. Creation of self-sensing samples. Upon reaching a certain saturation degree (designated or randomized), the prismatic sample was fractured into two pieces in three-point bending using a DARTEC

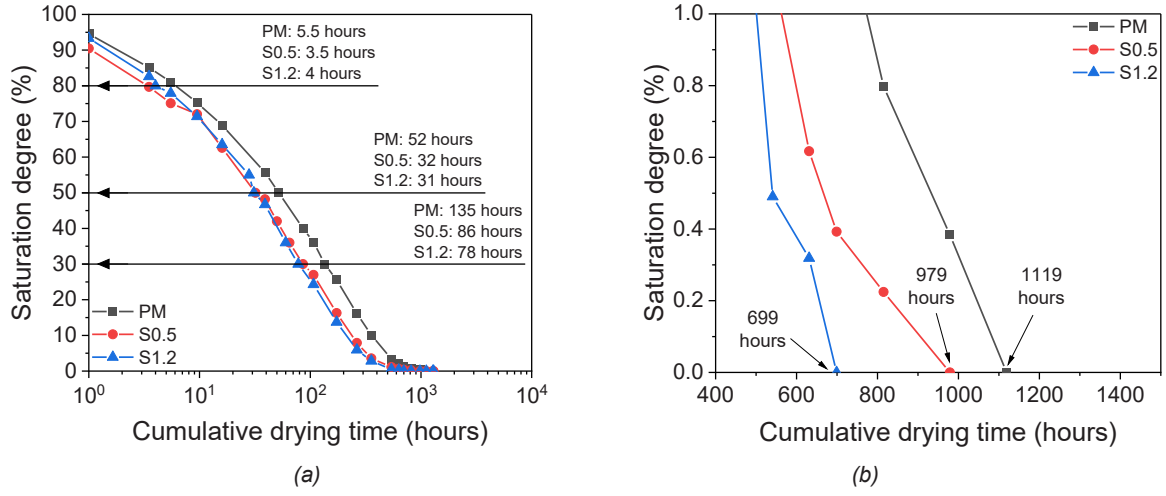

Fig. 2. Monotonic drying process at 60°C and 5% RH: (a) full record of the drying process; (b) detailed record at the final drying times for the determination of the mass equilibrium.

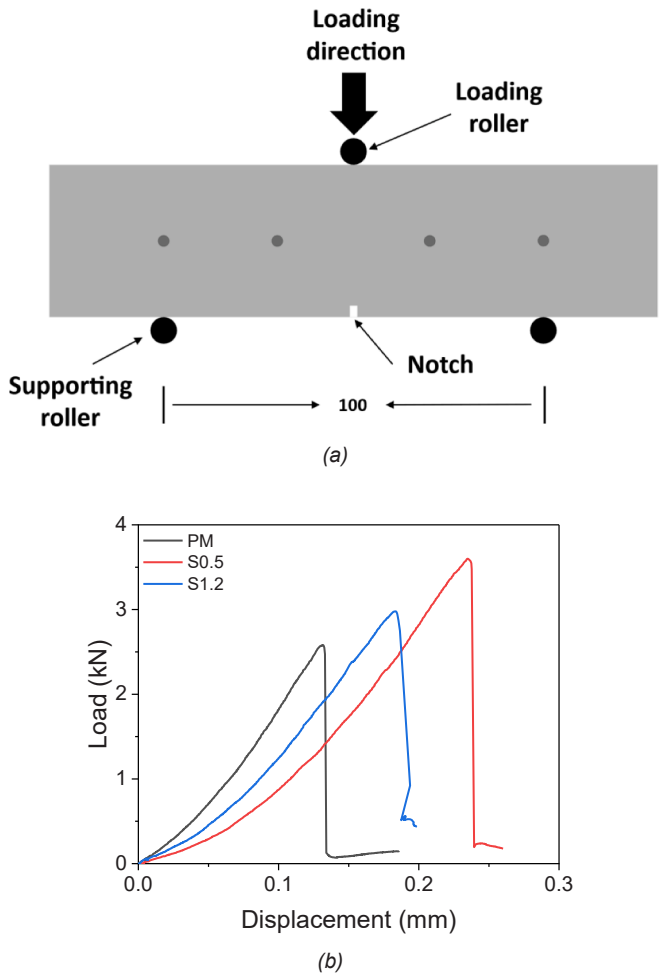

Fig. 3. Creation of the pieces for self-sensing tests: (a) configuration of three-point bending for the creation of half-prismatic pieces (b) load-displacement response of the prismatic samples exhibiting a brittle manner of failure.

(INSTRON, Buckinghamshire, UK) loading frame. A notch of 2 mm wide and 3 mm deep was created at the mid-span of the prismatic sample by a handsaw (Fig. 3a). The rollers had a diameter of 10 mm and a length of 45 mm, and the distance between the supporting rollers was 100 mm. The loading rate was 55 N/s as defined in BS EN 196–1. The load-displacement response for each sample was recorded in Fig. 3b. After a short "bedding in" process, the load-displacement response for all samples exhibited a linear behaviour, followed by the occurrence of the major crack at the peak load and finally fractured into two pieces in a brittle manner of failure. This suggests that the three-point bending configuration had marginal influence on the strength and the fibre-matrix bonding of the two pieces, indicating that the two pieces can be legitimately used for further experiments of self-sensing under uniaxial compression.

2.2.2.2. Self-sensing at designated saturation degrees. Self-sensing tests were then performed on the pieces of samples created following the three-point bending. Prior to loading, the surface of the sample was wiped with paper towel to minimize the influence of surface moisture on the measurement of volumetric impedance. The loading configuration complied with BS EN 196–1, where the compression rig had both a loading platen and a supporting platen with a contact area of 40 × 40 mm (Fig. 4a and b).

For self-sensing at designated saturation degrees, to understand the behaviour at a wide range of stresses, monotonic compression was employed where the load increased from 0 to around 72 kN (a stress of around 45 MPa). Displacement control was applied where the loading rate was 0.1 mm per minute. During self-sensing, the loading was paused at each 0.1 mm of the increase in displacement for the impedance measurement to be carried out (Fig. 4a). During the pause, the displacement control makes the loading platen fixed at certain position hence the material would have a slight reversal of stress and deformation. Therefore, each duration of pause was limited to less than 45 seconds to minimize the reversals so that the measured impedance can be reliably corresponded to the recorded stress. In comparison, load control (i.e., fixing at a constant load) was not employed because the deformation of the hardened cementitious matrix would increase over time if a persistent stress was applied on it. This behaviour of material creep can become worse with the increasing stress and even can cause earlier or unexpected material failure. Therefore, displacement control was preferable to enable wide range of behaviour in stress to be properly interpreted.

Samples were connected to a PSM 3750 impedance spectrometer (Newtons4th, Leicester, UK) via coaxial leads with crocodile clips (Fig. 4a). During the pause of the loading, two-point impedance measurement was performed by shorting the WE (working electrode) to the W*R* (working electrode reference) and the CE (counter electrode) to the CR (counter electrode reference) (Fig. 4b). The WE and W*R* injected the current and measured the voltage respectively, while the CE and CR measured the current and voltage respectively. This method eliminated the leakage current and the inductive loop which originally resulted from the limited input impedance of the internal circuit of the impedance spectrometer under a four-point configuration [94]. This method also allowed the capacity of the measurement to be maximized in terms of both the impedance magnitude and frequency range [95]. The maximum voltage was configured at the amplitude equivalent to an RMS of 707.107 mV. The frequency had a range of 10 Hz – 10 MHz. Logarithmic sweeping mode was employed with 10 points per log cycle (i.e., 60 points in total). The load and displacement were monitored through a digital interface (INSTRON, Buckinghamshire, UK) at a constant measuring frequency of 10 Hz (Fig. 4a).

2.2.2.3. Self-sensing at randomized saturation degrees. For self-sensing at randomized saturation degrees, cyclic compression was employed after the samples were exposed to the outside environment for 3 days without the knowledge of moisture content. The loading range was 0–10.2 kN (or a stress of 6.375 MPa), which was around 15% of the maximum load in self-sensing at designated saturation degrees. This is to understand the self-sensing behaviour after the random moisture exchange between the environment and the samples, which will frequently happen on site during service life of the sensors. Load control was employed because at such a relatively low stress range the influence of material creep on the impedance measurement can be marginal. The configurations of impedance measurement and load-displacement recording were the same as in Section 2.2.2.2 (Fig. 4a and b).

2.2.3. Physical meanings of resistance and reactance

The AC impedance, as a complex number, has the following formalism:

$$Z(\omega) = Z'(\omega) - jZ''(\omega) \tag{3}$$

where $j = \sqrt{-1}$, ω is the angular frequency (unit in radians per second) which equals to $2\pi f$ and f the frequency (unit in Hz), $Z'(\omega)$ the real part of the impedance which is the resistance R, and $Z''(\omega)$ the imaginary part of the impedance which is the capacitive reactance X.

A hardened cementitious material is semi-conductive, porous, and heterogenous with numerous solid-liquid interfaces. Under the excitation of the AC electric field through a series of frequencies, complex conduction and dielectric activities can take place both at the solid-liquid interfaces as surface effects, and in the conductive components (i.e., pore fluid, carbon fibres) as bulk effects [39,96,97], which can be

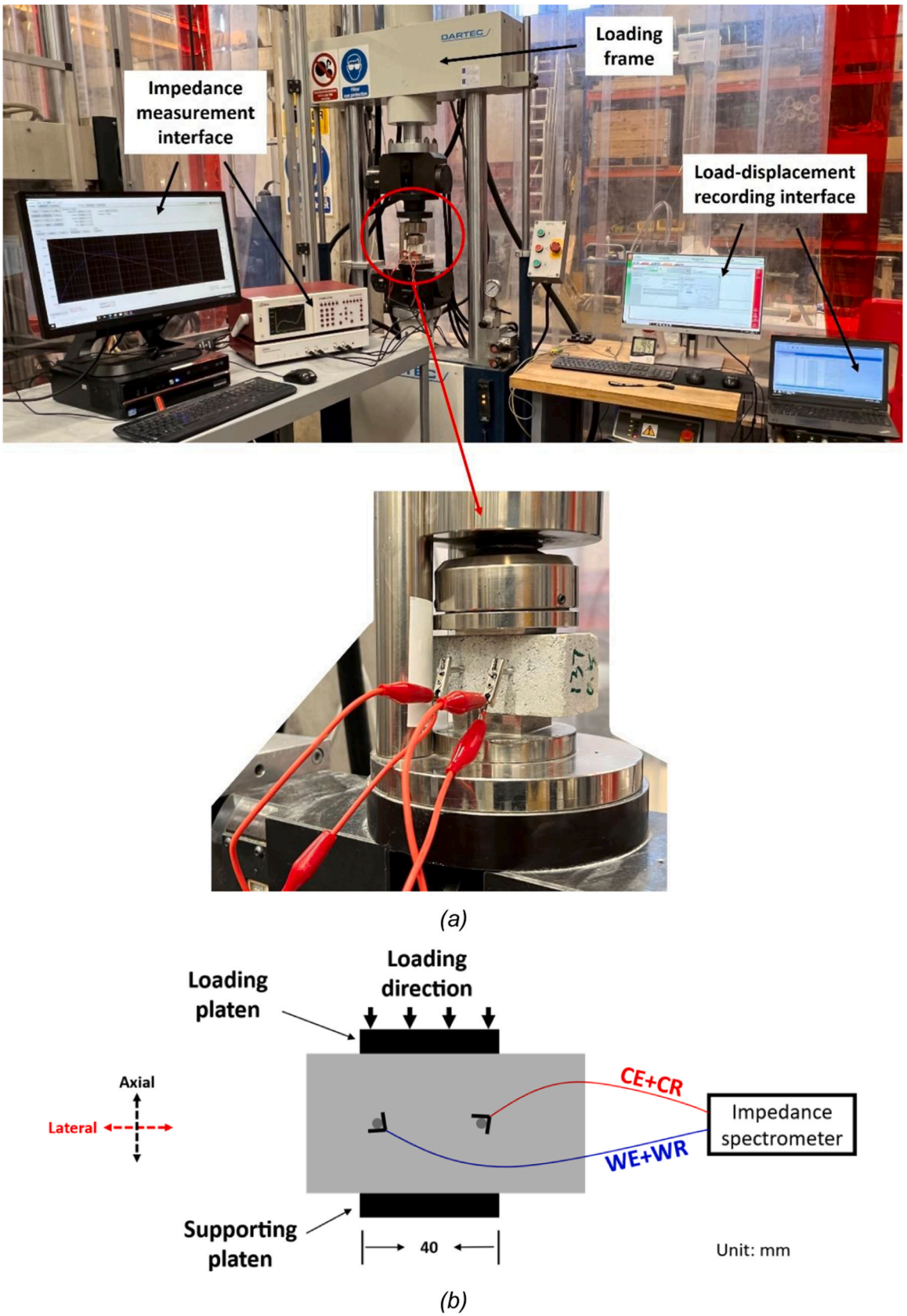

Fig. 4. Self-sensing of uniaxial compression: (a) photograph of the experimental setup (b) schematic illustration of the loading and data acquisition setups, CE refers to counter electrode, CR refers to counter electrode reference, WE refers to working electrode, W*R* refers to working electrode reference.

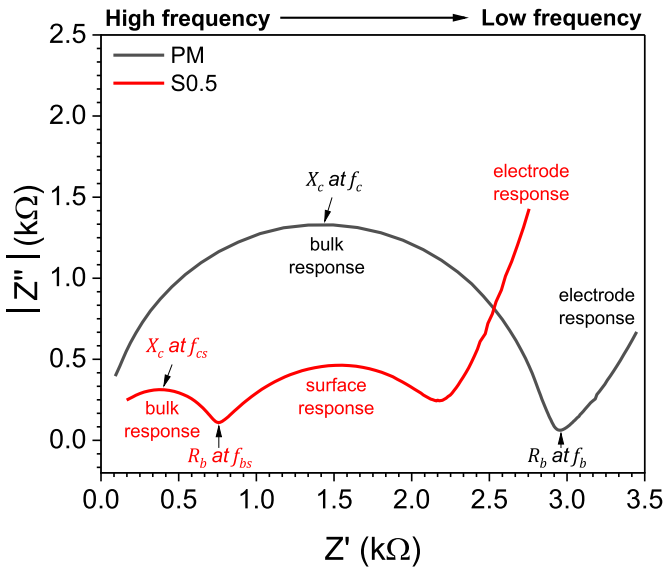

Fig. 5. Characteristics of the Nyquist plot of plain mortar and cement-based sensor (water-saturated PM and S0.5 at the curing age of 97 days as an example). The frequencies of R_b for plain mortar and the sensors are marked as f_b and f_{bs} respectively, while the frequencies of X_c for plain mortar and the sensors are marked as f_c and f_{cs} respectively.

differentiated on the Nyquist plot. Using two-point measurement, the Nyquist plot of a hardened plain mortar is comprised of two distinctive responses: the bulk response and the electrode response (Fig. 5). For cement-based sensors, the addition of carbon fibers into the mortar matrix results in the emergence of the surface response (i.e., the dielectric polarization at the interface of fibre surface-pore fluid) between the bulk and the electrode responses at intermediate frequencies (Fig. 5).

The most consistent parameters, bulk resistance (R_b), and characteristic reactance (X_c), can be extracted from the Nyquist plot, which are consistent parameters for sensing stress. The bulk resistance (R_b) quantifies the collective contributions of the ionic conduction through the pore fluid, electronic conduction through the carbon fibres, and the energy dissipation process of dielectric relaxations [40,98,99]. It resides at the intersections of the time constants where a transitional process occurs, that, the surface effect diminishes and the bulk response becomes dominant [72,100]. For plain mortar, R_b is acquired at the intersection of bulk and electrode responses. While for cement-based sensor, R_b is picked up at the intersection of bulk and surface responses (Fig. 5). The characteristic reactance X_c estimates the capacitance (or the ability of energy storage) of the bulk system [101]. It can be obtained at the peak point of the bulk arc where the highest absolute value of imaginary impedance $Z''(\omega)$ at frequencies 1 kHz – 10 MHz is reached (Fig. 5). In this study, the absolute values of the imaginary impedance $|Z''(\omega)|$ and the characteristic reactance X_c were used for the ease of expression and calculation, as presented in the vertical axis of the Nyquist plot in Fig. 5. The frequencies of R_b and X_c for both the plain mortar and the sensor have been denoted in Fig. 5.

The piezoresistivity and piezopermittivity can be evaluated through fractional change in bulk resistance R_b (FCR_b), and fractional change in characteristic reactance X_c (FCX_c), which are calculated using Eqs. 4 and 5, respectively:

$$FCR_b = \frac{R_{bs} - R_{b0}}{R_{b0}} \times 100\% \quad (4)$$

and

$$FCX_c = \frac{X_{cs} - X_{c0}}{X_{c0}} \times 100\% \quad (5)$$

where the R_{bs} and X_{cs} are the bulk resistance and characteristic reactance at a certain stress level, R_{b0} and X_{c0} the bulk resistance and characteristic reactance of the sensor in pristine condition (i.e., without stress).

2.2.4. Evaluation on the pore structure

In this study, water saturated samples were dried under 60°C over a period for self-sensing at designated saturation degrees. Unlike other studies where dried samples were re-saturated for a certain period of time [59,67], drying from saturation provides accurate determination of moisture content by avoiding the hysteresis phenomenon. However, although 60°C is a relatively lower drying temperature in comparison to 105°C which has been a popular way [92,102,103], decomposition of hydration products occurs and the pore structure can be damaged [104, 105]. Understanding the influence of drying on the microstructure can help to critically evaluate the interconnected self-sensing mechanism of the changing moisture and fibre contents. Therefore, the porosities before and after drying were compared. The porosity after drying was calculated by:

$$Water\ porosity = \frac{M_0 - M_e}{\rho_{20} V_p} \times 100\% \quad (6)$$

where M_0 was the mass (unit in g) of the samples at zero drying time, M_e the mass at the condition of mass equilibrium as defined in Section 2.2.1, ρ_{20} the density of water at 20°C (unit in g/cm^3), V_p the total volume of the sample (unit in cm^3).

The porosity before drying was obtained via MIP. Samples from the same batch were fractured by three-point bending. Then, fragments were taken at the fractured location, which were between the electrodes where the impedance was measured. The fragments were then put under vacuum-drying until the condition of mass equilibrium was reached. MIP was then undertaken on Pascal 140 and Pascal 440 (Thermo Fisher Scientific Inc, Milan, Italy) machines. For all fragments, the intrusion pressure was increased from 0 to 400 MPa and the Hg contact angle was 140°.

2.2.5. Polarized light microscopy

In a cement-based sensor, the liquid filled pores and the carbon fibres are the most important conductive components for ionic and electronic conduction, respectively. To understand the relationships among the mortar matrix, the carbon fibres, and the pores, polarized light microscopy was used. Polished thin sections were processed by Hands on Thin Sections Ltd (Worcestershire, UK), which were examined under cross polarized transmitted and incident light using a Leica DM750 P microscope (Leica Microsystems Ltd, Milton Keynes, UK). The objective lens had a 5-time magnification where the air voids, hollow-shell pores, larger capillary pores, and the carbon fibres can be visually confirmed.

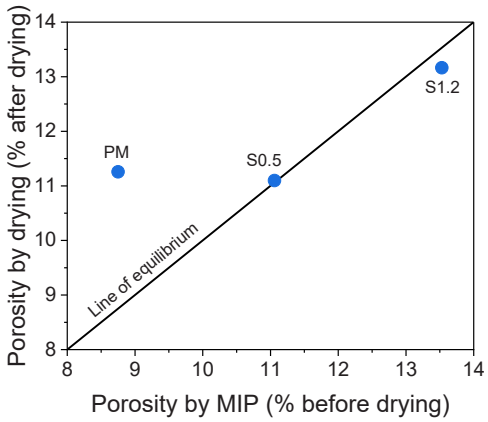

Fig. 6. Comparison between the porosities before and after drying.

3. Results and discussions

3.1. Microstructural characterization

3.1.1. Water porosity and mercury porosity

In Fig. 6, the porosity after drying (i.e., porosity by drying) has been plotted against the porosity before drying (i.e., porosity by MIP). Using the same scale on vertical and horizontal axes, the 45° line represents equilibrium between porosity before and after drying. The porosities by MIP increased as the fibre content increases, which were 8.75%, 11.06%, and 13.53% for PM, S0.5, S1.2, respectively. This result was consistent with previous studies [55,57,72] which was ascribed to the increased degree of fibre agglomeration, the increased number of fibre-matrix interfaces, and the increased air bubbles during mixing while increasing the fibre content. The porosities by drying for PM, S0.5, and S1.2 were 11.23%, 11.06%, 13.16%, respectively. It can be seen that after drying, the porosity of PM increased by 2.48% (Fig. 6). Also, previous studies showed that for cement pastes, the porosity by oven drying can be higher than the porosity by MIP regardless of the cement type [103,104]. This corresponds to the decomposition of hydration products (i.e., ettringite) under high drying temperature with the associated pore structure collapse, and the water molecule can widen up the pore network due to being a stronger polar liquid expanding the volume during evaporation [105,106]. In comparison, S0.5 and S1.2 both had marginal changes in porosities before and after drying (Fig. 6). This suggests that the sensors are more resistant to microstructural damages during drying under elevated temperatures, which can be ascribed to the fibre-matrix bonding based on previous studies where carbon fibre reinforced concrete exhibited lower extent of drying shrinkage [14,35,107,108].

3.1.2. Polarized light microscopy

Polarized light microscopy can reveal the relationship between the mortar matrix, the carbon fibres, and the pores. Under unpolarized light, one photograph was taken. Under polarized light, the thin section was rotated by 360° horizontally, during which 12 photographs were taken for the identification of the mixing components, where the materials would appear as different colours due to their optical anisotropy. For example, in Fig. 7a and b, the cement matrix, due to its large density, amorphous nature, and rough surface, appeared large continuous dark areas under both the unpolarized and polarized lights. The minerals appeared white under unpolarized light, whilst being able to change into different colours under polarized light depending on their surface roughness, light reflective ability, and the rotation angle. The regular-shaped, black needles are carbon fibres. The pores appeared white which was undiscernible from the minerals under unpolarized light (Fig. 7a) but can be visually confirmed if irregularly shaped dark areas (marked in red circles) were consistently spotted during the rotation due to allowing the polarized light to go through at all rotational angles (Fig. 7b).

In S1.2, the carbon fibres formed into bunches where physical contact points can be visually confirmed (Fig. 7b) forming continuous conductive pathways. In S0.5, the carbon fibres were distributed in the mortar matrix in a scattered manner (Fig. 7d) where fewer physical contact points were identified in comparison to S1.2. It can therefore be confirmed that S1.2 had better continuity of the electronic conduction pathway by the carbon fibres than S0.5. In S1.2, a few small pores can be found in the carbon fibre bunches which might be the fibre-matrix interfacial location or the air bubbles that came from mixing process, whilst some larger pores existed outside of the carbon fibre bunches (Fig. 7b). In S0.5, the pores were scattered throughout the mortar matrix which was similar to the distribution of the carbon fibres (Fig. 7d).

3.2. Complex impedance behaviour

3.2.1. Under increasing compressive stress

In Fig. 8, the complex impedances of plain mortar and cement-based sensor under various compressive stresses are presented as Nyquist plot. PM and S1.2 at 80% of saturation degree were selected as examples. The size of the arced bulk response of S1.2 was smaller than that of PM due to the addition of carbon fibres enhancing the conductivity and dielectric behaviour [71,99]. In Fig. 8, as the compressive stress increased from 0 to around 25 MPa, both the bulk responses of PM and S1.2 had reduced in size. The R_b (marked as red sphere) moved from the right to the left side and the X_c (marked as blue sphere) moved downwards. For PM, R_b reduced from 3.8 kΩ to around 2 kΩ and X_c reduced from 1.7 kΩ to 0.9 kΩ (Fig. 8a). For S1.2, R_b decreased from 1.7 kΩ to 1 kΩ and X_c decreased from 0.7 kΩ to 0.4 kΩ (Fig. 8b). This indicated that the resistance and reactance of the system had reduced (or the conductance and capacitance had increased) under a continuously increasing compressive stress, regardless of the fibre inclusion.

3.2.2. Under decreasing saturation degree

In Fig. 9, the impedance responses of plain mortar and cement-based sensors under the decreasing saturation degree were plotted. PM and S1.2 at their pristine condition before the application of any stress were presented as examples. As the water saturation degree reduced from 80% to 30%, the size of the bulk arcs of both PM and S1.2 had extended, with the associated movement of X_c upwards and R_b from left to right. For PM, R_b increased from 3.7 kΩ to 31 kΩ and X_c increased from 1.7 kΩ to 14 kΩ (Fig. 9a). For S1.2, R_b increased from 1.7 kΩ to 10 kΩ and X_c increased from 0.7 kΩ to 4.3 kΩ (Fig. 9b). This indicated that the reduction in moisture content led to the reduction of conduction and capacitance of the system regardless of the fibre inclusion, which was consistent with previous studies [55,72].

3.3. Self-sensing at randomized saturation degrees

After the internal moisture of the sample being passively exchanged with the outside environment for three days, self-sensing performance was examined in the form of cyclic compression and the results are plotted in Fig. 10. The stress increased from 0 to 6.375 Mpa and the compressive process was repeated by three cycles, during which the impedance was measured (Fig. 10a). Performances of piezoresistivity and piezopermittivity were presented in Fig. 10b and c, respectively. In general, both the FCR_b and FCX_c decreased with the increasing compressive stress during loading, whilst increased with the decreasing stress during unloading, regardless of the fibre contents (Fig. 10b and c). In each cycle, both the FCR_b and FCX_c reached their maximum values at the maximum stress 6.375 MPa. For all testing samples, the maximum values of FCR_b and FCX_c changed negligibly when compared amongst each compressive cycle. For example, from cycle one to cycle three, the maximum FCR_b for S0.5 was −30.4%, −31%, and −31.1%, respectively (Fig. 10b). The maximum FCX_c for S1.2 was −65.9%, −66.6%, and −66.6%, respectively (Fig. 10c). This indicates good sensing repeatability for all samples regardless of the fibre inclusion, which can be ascribed to the low stress levels. More importantly, the maximum values for FCR_b and FCX_c increased with the increasing fibre content. For example, in cycle one, the maximum FCR_b for PM, S0.5, and S1.2 was −1.1%, −30.4%, −45%, respectively, while the maximum FCX_c for PM, S0.5, and S1.2 was −9.6%, −48.1%, and −65.9%, respectively.

The sensing recoverability, which is the sensor's ability to recover its pristine electrical behaviour upon finishing the three compression cycles at load release, was also marked in Fig. 10b and c. For PM, S0.5, and S1.2, the sensing recoverability was −0.1%, −3.3%, and −8.6% respectively by FCR_b (Fig. 10b). The sensing recoverability characterized by FCX_c for PM, S0.5, and S1.2 was −1.4%, −14.8% and −24.6% respectively (Fig. 10c), which were all higher than that by FCR_b (Fig. 10b). It is therefore evident that the sensing recoverability reduced

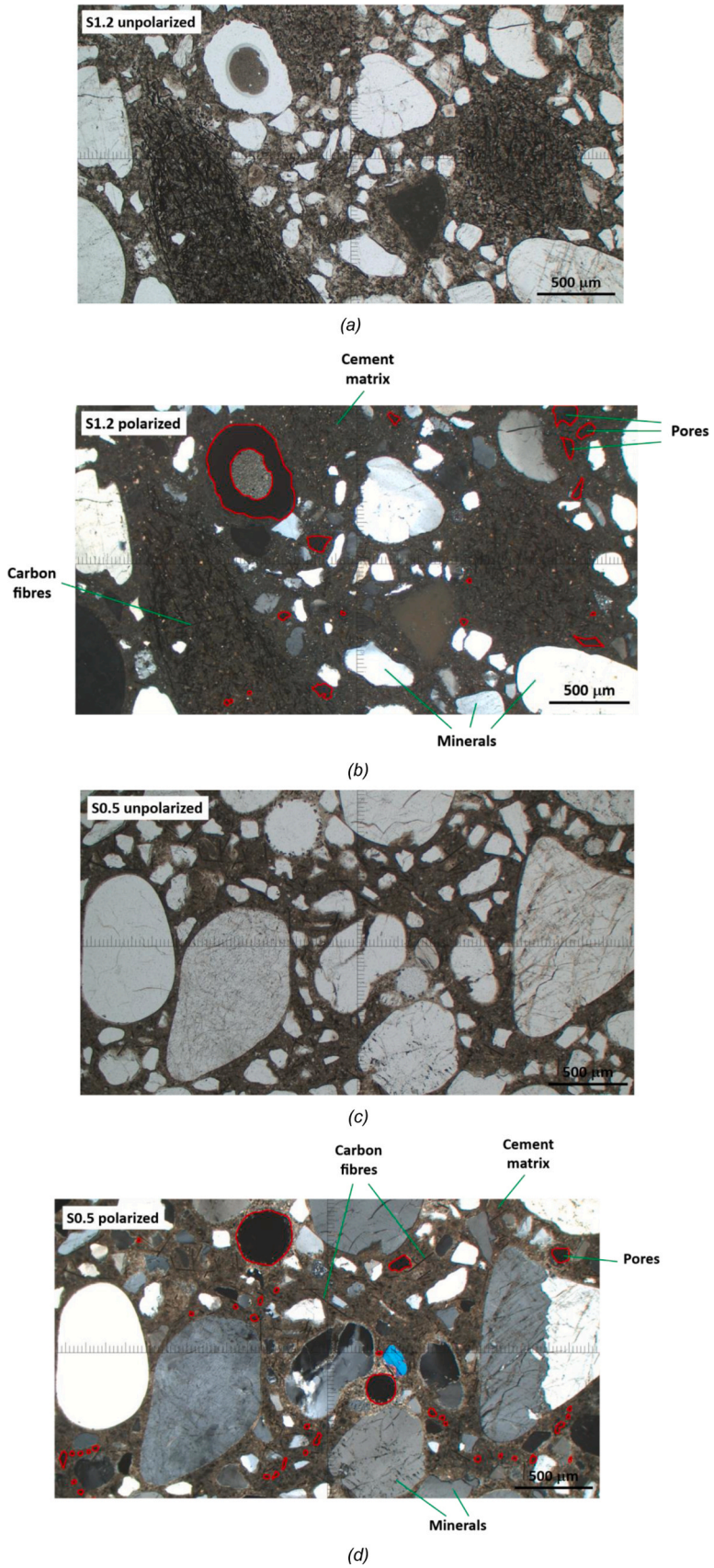

Fig. 7. Photograph of the mixing components in sensor's matrix under microscopy: (a) S1.2 under unpolarized light (b) S1.2 under polarized light (c) S0.5 under unpolarized light (d) S0.5 under polarized light.

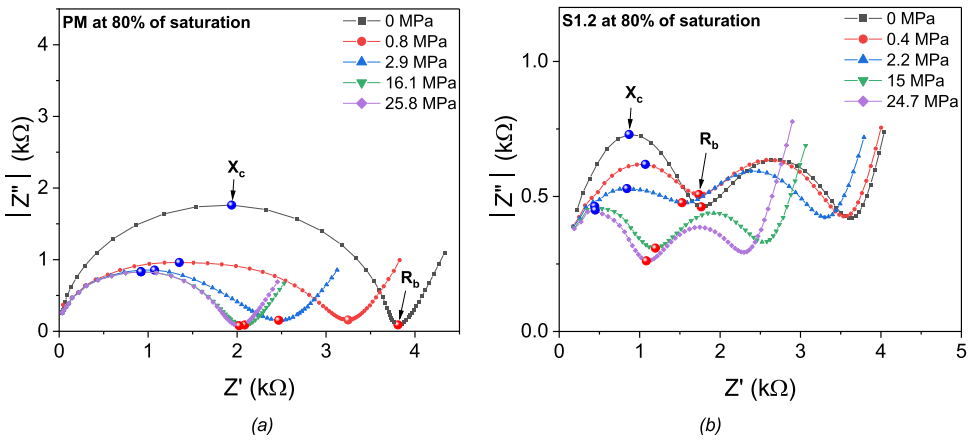

Fig. 8. Impedance response of plain mortar and cement-based sensor under monotonic compression: (a) PM at 80% of saturation (b) S1.2 at 80% of saturation.

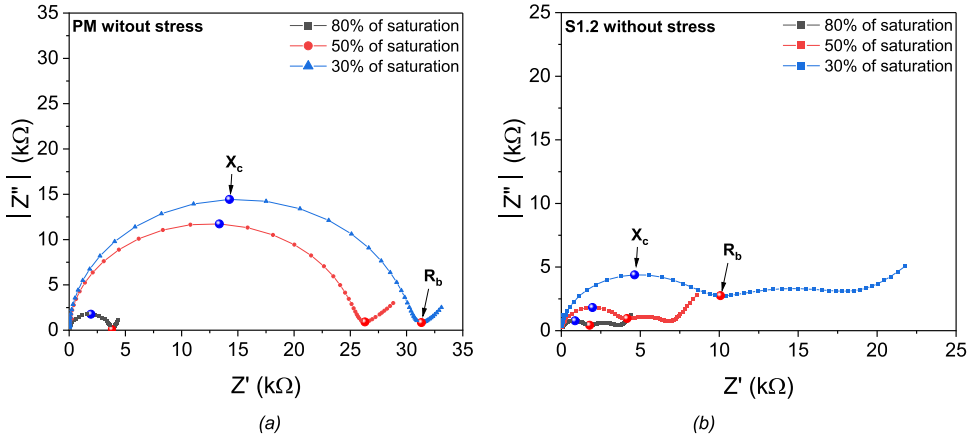

Fig. 9. Impedance response of plain mortar and cement-based sensor under decreasing saturation degree: (a) PM without stress (b) S1.2 without stress.

with the increasing fibre content.

The sensing linearity and sensitivity can be extracted by linearly fitting the relationships between FCR_b (or FCX_c) and stress during the load increase in cycle one (Fig. 11). The linear fitting was performed at stress range of 0.125 – 6.375 MPa, where the condition at zero stress (i.e., the baseline condition) was excluded because the natural brittleness of cementitious materials can cause irrecoverable impedance at the load release (Fig. 10b and c).

The linear fitting was successful for PM and S1.2 by the characterization of both the FCR_b (Fig. 11a) and FCX_c (Fig. 11b) with high R^2 values. However, the linear fitting failed for S0.5, presenting lower R^2 values of 0.62 for FCR_b (Fig. 11a) and 0.57 for FCX_c (Fig. 11b). It can therefore be postulated that the sensing linearity is dependent on the dominance of the conductive components. It has been identified in our previous study that the conduction of electricity in PM is ionically dominant by the liquid filled pores, and the S1.2 is electronically dominant by the carbon fibres. Whilst S0.5 had the same moisture dependence of conductivity as PM indicating that the electronic conduction by the carbon fibres is not strong enough hence the S0.5 is still ionically dominant [72]. Also, referring back to Fig. 7, the electronically conductive pathway through the carbon fibres of S1.2 exhibited sound continuity (Fig. 7b), whilst S0.5 had scattered distributions of both the pores and carbon fibres (Fig. 7d) presenting a lesser continuity of electronic conduction pathway in comparison to that of S1.2.

The sensing sensitivity was quantified by the gauge factor (GF) in Fig. 11, which is the absolute value of the slope of the linear fit. PM had relatively low GF values which can be negligible presenting minimized stress self-sensing functionality. For the sensors, the GF by both the FCR_b and FCX_c increased with the increasing fibre content. For example, by FCR_b, S1.2 had a GF of 4.2% MPa^{-1} while S0.5 had a GF of 4% MPa^{-1} (Fig. 11a). The increase of fibre content provided increased numbers of electronically conductive channels (i.e., contact conduction, tunnelling conduction) and fibre-matrix interfaces, which led to the enhanced activities during loading and unloading (e.g., fibres touching and separating, and fibres push-in and pull-out), hence the enhanced changes in the impedance per unit stress [88,109–112]. In addition, the GFs of FCX_c were higher than that of FCR_b regardless of the fibre inclusion. For example, for S1.2, the GF was 4.2% MPa^{-1} by FCR_b (Fig. 11a), and the GF was 4.8% MPa^{-1} by FCX_c (Fig. 11b). It is therefore evident that the FCX_c was a more sensitive indicator for sensing stress than FCR_b at stresses 0–6.375 MPa after the moisture of the sensors was passively exchanged with the environment for three days.

3.4. Self-sensing at designated saturation degrees

3.4.1. Electrically dominant sensor: S1.2

The self-sensing behaviour of S1.2 at designated saturation degrees, 80%, 50%, and 30%, was presented in Fig. 12. It has been identified in our previous study that the conduction of electricity in S1.2 was electronically dominant with low moisture dependence [72], exhibiting sound continuity of electronic conduction pathways by the carbon fibres in the sensor's matrix (Fig. 7b). Although having dried under 60°C for a controlled water saturation degree, the load-displacement response of S1.2 at each saturation degree showed consistent behaviour (Fig. 12a). This can correspond to what was found in Fig. 6 where the porosity of S1.2 changed marginally after drying: it is possible that the C-S-H gel,

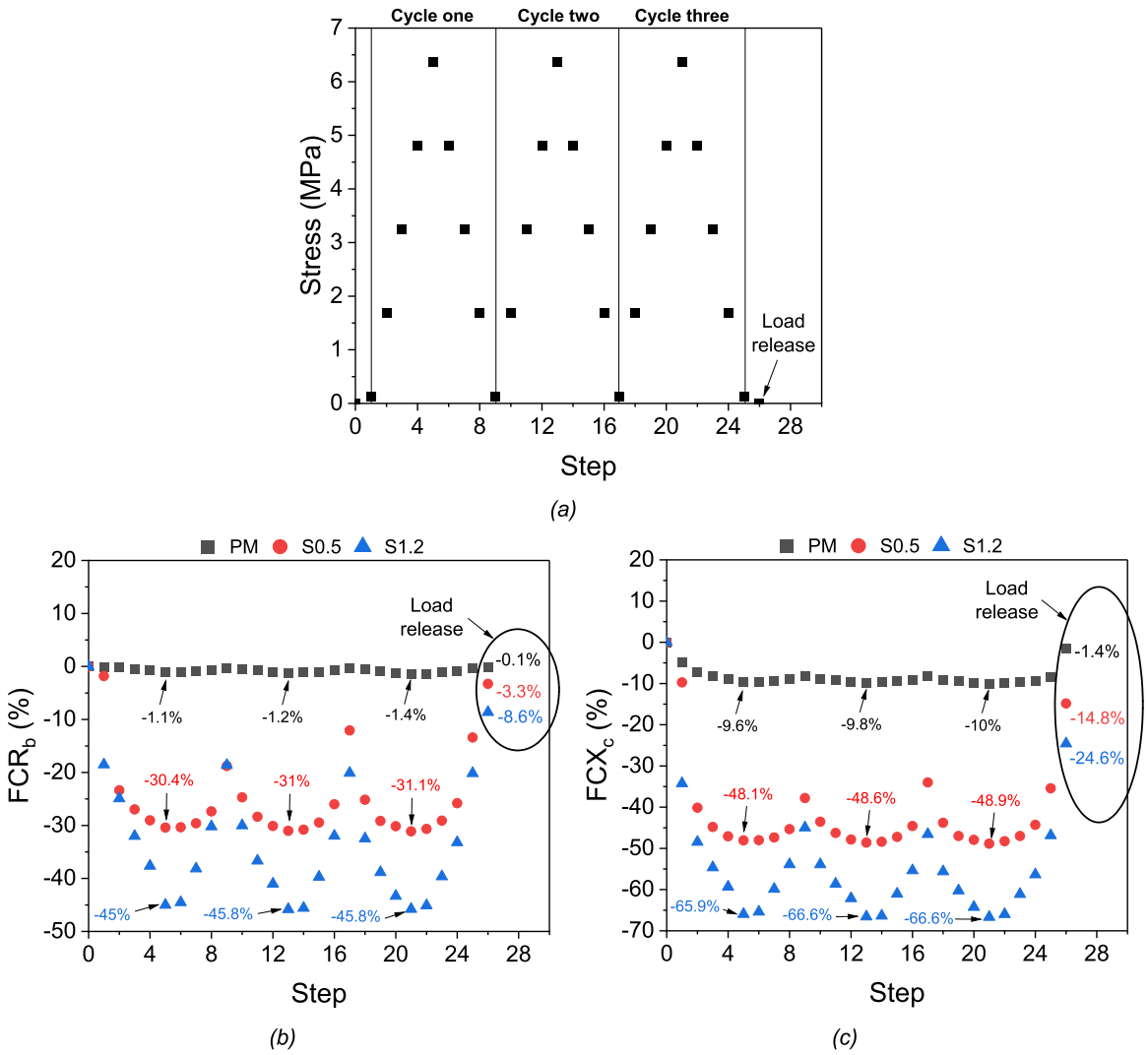

Fig. 10. Self-sensing behaviour at random saturation degrees of PM, S0.5, and S1.2 in the form of cyclic compression: (a) Recorded stress at each measurement step (b) piezoresistivity using FCR_b (c) piezopermittivity using FCX_c.

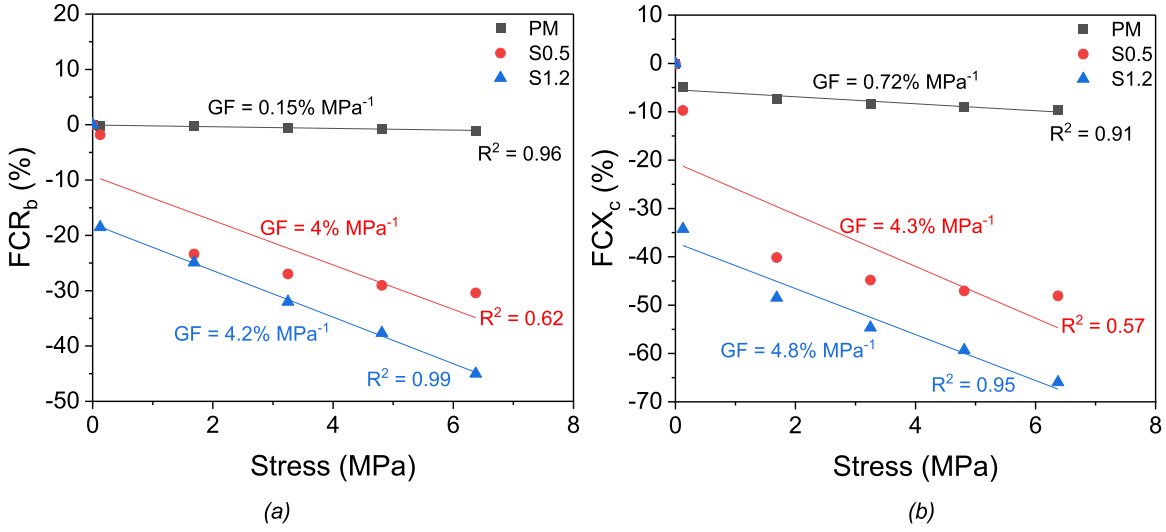

Fig. 11. Correlations between electrical properties and stress through the self-sensing behaviour during the load increase in cycle one: (a) FCR_b vs stress (b) FCX_c vs stress.

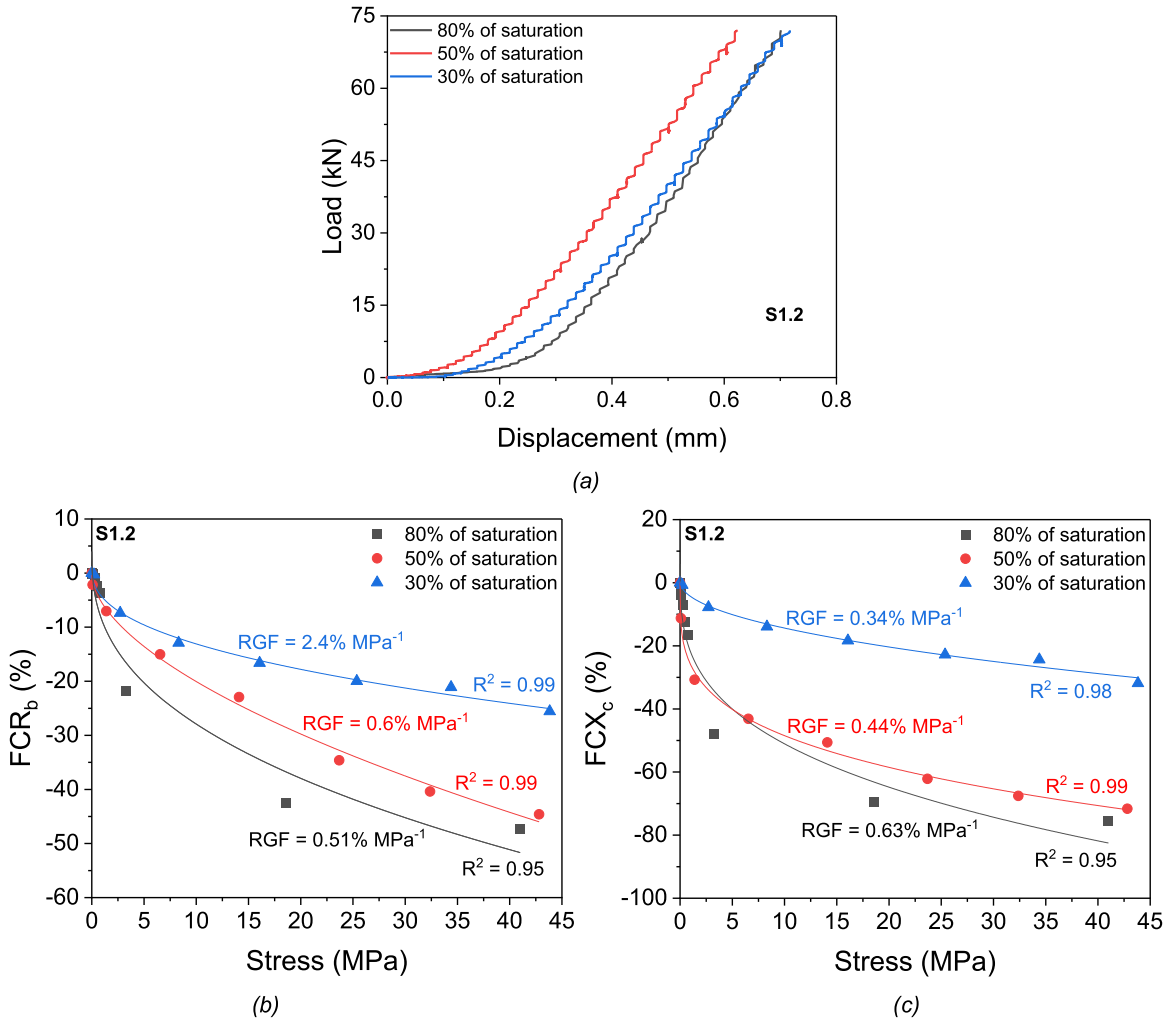

Fig. 12. Self-sensing behaviour of S1.2 at saturation degrees 80%, 50%, and 30% of S1.2 in the form of monotonic compression: (a) load-displacement record (b) piezoresistivity using FCR_b (c) piezopermittivity using FCX_c.

which is the main phase responsible for the material strength, was negligibly influenced under 60°C because the de-hydration temperature of C-S-H can be as high as 105°C [104,113].

Regardless of the stress level, both the magnitude of FCR_b and FCX_c decreased with the decreasing saturation degree due to the weakened ionic conduction (Fig. 12b and c). Regardless of the saturation degree, both FCR_b and FCX_c decreased with the increasing stress (Fig. 12b and c). Due to covering a wide range of stresses from 0 to around 45 MPa, the relationship between the electrical properties and stress obeyed the power law with reducing gradient, which can be fitted by the following expression:

$$FCR_b \ (or\ FCX_c) = n + m\sigma^p \tag{7}$$

where the σ is stress in MPa, and the n, m, and p are the fitting coefficients.

The reducing gradient with the increasing stress indicated the reducing sensing sensitivity. This can be ascribed to the accumulation of microcracks [7] which increased with stress. The sensing sensitivity, which is the gauge factor (GF), can be described by the absolute value of the derivative of the power law curve as shown in Eqs. 8 and 9:

$$GF = \left|\frac{d(FCR_b)}{d\sigma}\right| = \left|pm\sigma^{p-1}\right| \tag{8}$$

or

$$GF = \left|\frac{d(FCX_c)}{d\sigma}\right| = \left|pm\sigma^{p-1}\right| \tag{9}$$

where the unit for GF is MPa^{-1}. In this case, the residual gauge factor (RGF), which was the GF at the maximum stress 45 MPa of the fitted power law curve, was used to represent the sensor's sensing sensitivity.

In Fig. 12b and c, the power law fitting was successful with high R^2 values. While decreasing the saturation degree from 80% to 30%, the RGF increased from 0.51% to 2.4% MPa^{-1} by FCR_b (Fig. 12b). For the piezoresistivity, the bulk resistance R_b reflects any changes in the conductive pathways under stress. For S1.2 whose conduction of electricity is electronically dominant, the changes in the conductive pathways over stressing were thus dominated by the changes in contact conduction by physically contacted carbon fibres and the tunnelling transmission by the hopping of the electrons/holes between adjacent fibre tips if within the tunnelling range [8,111,114]. It is certain that while decreasing the saturation degree, the ionic conduction weakened but the contact conduction remained intact. At higher saturation degrees, the hopping of electrons/holes between adjacent fibre tips was hindered due to being submerged in pore fluid. While the saturation degree was decreasing, fibre tips were gradually exposed hence the tunnelling transmission of electrons/holes were progressively enhanced (Fig. 13). Due to the electronically dominant conductivity of S1.2, such enhancement of tunnelling transmission was strong enough to prevail the reducing ionic conduction. Therefore, the RGF of FCR_b increased

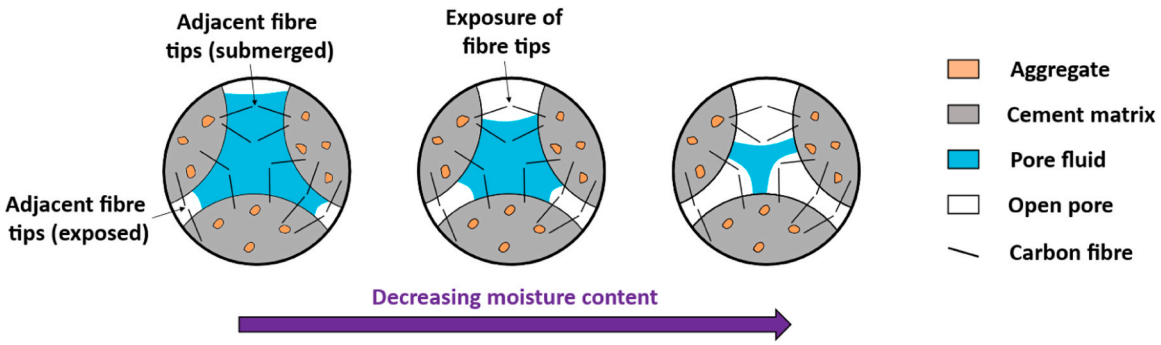

Fig. 13. Schematic illustration for the enhancement of tunnelling effect by the exposure of originally submerged adjacent fibre tips as the moisture content reduces.

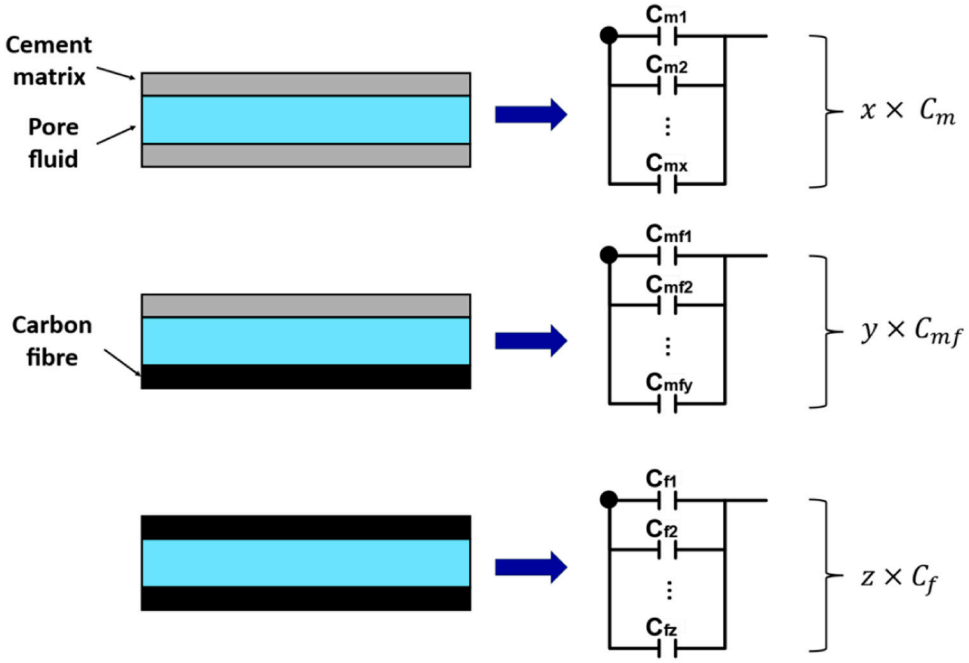

Fig. 14. Solid-liquid phases to construct layered capacitor in a cement-based sensor: C_m is the cement-pore fluid-cement layered capacitor, C_{mf} is the cement-pore fluid-fibre layered capacitor, C_f is the fibre-pore fluid-fibre layered capacitor, x, y, and z are their numbers, respectively.

with the decreasing saturation degree due to the enhanced tunnelling effect for the response to stress (Fig. 12b).

In contrast, while decreasing the saturation degree from 80% to 30%, the RGF decreased from 0.63% to 0.34% MPa^{-1} by FCX_c (Fig. 12c). For piezopermittivity, the characteristic reactance X_c reflects any changes in the system capacitance under stress. The characteristic reactance X_c was obtained within the frequency range 1 kHz – 10 MHz, where the Maxwell-Wanger type interfacial polarization took place. Therefore, the layer model can be used to explain the reason why RGF decreased with the decreasing saturation degree using FCX_c as indicator [71,98,115]. In S1.2, there exists layered capacitors, which is comprised of solid and liquid phases, in three forms: cement-pore fluid-cement, cement-pore fluid-fibre, and fibre-pore fluid-fibre (Fig. 14).

The increase of solid-liquid interfaces and porosity would increase the capacitance of a cementitious material [39,72,100]. Based on this principle, in Fig. 14, the layered capacitors were connected together parallelly for the contribution of system capacitance C, which can be expressed as:

$$C = xC_m + yC_{mf} + zC_f \tag{10}$$

where C is the system capacitance of S1.2, C_m the capacitance of one unit of "cement-pore fluid-cement" layered capacitor, C_{mf} the capacitance of one unit of "cement-pore fluid-fibre" layered capacitor, and C_f the capacitance of one unit of "fibre-pore fluid-fibre" layered capacitor, x, y, and z are the number of the unit capacitors C_m, C_{mf}, C_f, respectively.

Based on Eq. 10, it can be proposed that evaporation of pore fluid between solid layers can be analogous to the reduction of the number of the layered unit capacitors, which equals to the decrease in the values of x, y, and z, hence the total system capacitance C (Fig. 14).Therefore, it is proposed that the decreased RGF by FCX_c with the decreasing saturation degree was because of the decreased number of capacitive channels for the response to stress.

Comparing piezoresistivity to piezopermittivity, at a higher saturation degree 80%, the RGF of FCR_b was 0.51% MPa^{-1} (Fig. 12b), being lower than that of FCX_c which was 0.63% MPa^{-1} (Fig. 12c). At lower saturation degrees 50% and 30%, the RGF of FCR_b was 0.6% MPa^{-1} and 2.4% MPa^{-1} respectively, being higher than that of FCX_c which was 0.44% MPa^{-1} and 0.34% MPa^{-1} respectively. It can therefore be concluded that while conducting stress self-sensing, for an electronically dominant cement-based sensor like S1.2, the piezopermittivity is a more sensitive property at higher saturation degrees, whilst the piezoresistivity can be more sensitive at lower saturation degrees. This is reasonable because the capacitance of the system was positively related

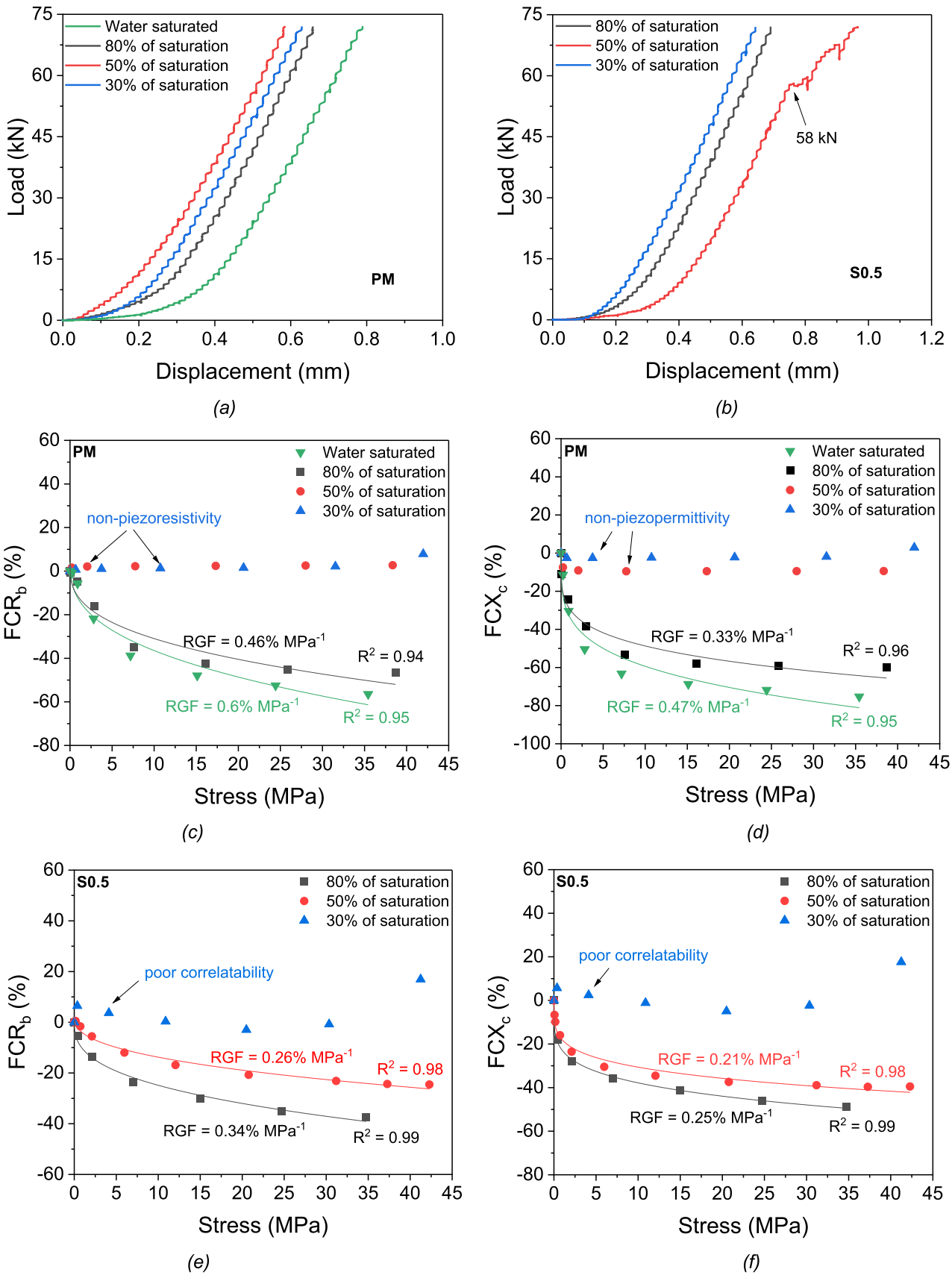

Fig. 15. Self-sensing behaviour of PM and S0.5 at saturation degrees 80%, 50%, and 30% of S1.2 in the form of monotonic compression: (a) load-displacement record of PM (b) load-displacement record of S0.5 (c) piezoresistivity using FCR_b for PM (d) piezopermittivity using FCX_c for PM (e) piezoresistivity using FCR_b for S0.5 (f) piezopermittivity using FCX_c for S0.5.

to the saturation degree (Fig. 9) which prevailed at higher saturation degrees hence a more sensitive response of piezopermittivity. Whilst at lower saturation degrees, the contact conduction stayed consistent, the capacitance of the system had reduced, but the strength of tunnelling transmission prevailed (Fig. 13), hence a more sensitive resistance-based response.

3.4.2. Ionically dominant sensor: S0.5

It was confirmed in our previous work that the conduction of electricity in S0.5 shared the same moisture dependence of conductivity as PM, exhibiting an ionically dominant nature [72]. Also, in Fig. 7d, it can be identified that the carbon fibres in S0.5 had a scattered distribution, showing a poor continuity of electronic conduction pathways. Therefore, in this section, the stress sensing behaviour of S0.5, was analysed together with PM, where their sensing behaviours at various saturation degrees were plotted in Fig. 15. The load-displacement response of PM showed consistency at all saturation levels (Fig. 15a) despite of its widened pore structure (Fig. 6). The load-displacement response of S0.5 showed a decrease in gradient at loads from 58 to 72 kN at 50% of saturation degree (Fig. 15b). Because the porosity of S0.5 after drying changed negligibly (Fig. 6), and as mentioned above, the C-S-H gel was marginally influenced under 60°C, this change in gradient at higher stress levels can be corresponded to other reasons such as the poor fibre dispersion of the sample (Fig. 6).

At higher water saturation degrees when changing from full saturation to 80% of saturation, the RGF of PM decreased both by the characterization of FCR_b and FCX_c (Fig. 15c and d). However, at the lower saturation degrees 50% and 30%, PM showed behaviours of non-piezoresistivity and non-piezopermittivity, where both the FCR_b and FCX_c changed marginally with the increasing stress (Fig. 15c and d). This proved that the moisture content is positively related to the sensing sensitivity of PM. At higher water saturation degrees, the increase in both FCR_b and FCX_c of PM with the increasing compressive stress can be attributed to the change of liquid filled closed pores into liquid filled open pores while loading, hence the increased ionic channels for the response to stress. In comparison, at lower saturation degrees 50% and 30%, although it is still possible for the ionic channels to increase with the increasing stress, the total number of ionic channels were not sufficient enough for the production of pressure sensitive responses due to low moisture content and the blockage of open pores by microcracking prevailed, hence a marginal pressure sensitive response.

For S0.5, the stress self-sensing behaviour was consistent between the characterizations of FCR_b and FCX_c. At 30% of water saturation, poor correlatability between stress and fractional values was presented where the power law did not fit (Fig. 15e and f). At 80% and 50% of saturations, S0.5 showed decent stress self-sensing performance, where the RGF decreased with the decreasing saturation degree (Fig. 15e and f) both by FCR_b and FCX_c. The underlying mechanism of such self-sensing performance can be explained by the comparison between S0.5 and S1.2. When decreasing the saturation from 80% to 50%, the decreased RGF by both the FCR_b and FCX_c was mainly resulted from the loss of moisture based on the ionically dominant nature of S0.5. Whilst at 30% of saturation, it can be proposed that the poor correlation can be attributed to the weak contact conduction, tunnelling transmission, and the ionic conduction. As presented above, the carbon fibres in S0.5 had a reduced continuity of contact conduction formed by the fibres in comparison to that in S1.2 (Fig. 7). Also, like in S1.2, the tunnelling transmission in S0.5 was enhanced with the decrease of saturation degree (Fig. 13). However, the enhancement was of a lesser extent due to larger distance between the fibres in S0.5 compared to S1.2. Moreover, the ionic conduction can be weak at such low water saturation. The above three mechanisms did not prevail the negative effects such as the blockage of conductive channels due to pore structure collapse whilst stressing. On top of that, the poor correlatability between stress and electrical properties can be considered as an ununiform alternation of conductive pathways over stressing, which can be associated with the ununiform dispersion of the carbon fibres in the mortar matrix.

Table 2
Sensing stability of cement-based sensors while reducing the saturation degree from 80% to 50%.

Characterization indicator of RGF	Sensor	Variation (%)
FCR_b	S0.5	-24
	S1.2	19
FCX_c	S0.5	-16
	S1.2	-30

For both the PM and S0.5, at all tested water saturations, piezoresistivity is more sensitive than piezopermittivity. For example, at 80% of saturation, the RGF of S0.5 was 0.34% MPa^{-1} by FCR_b (Fig. 15e), being higher than the RGF of 0.25% % MPa^{-1} by FCX_c (Fig. 15 f), which can be ascribed to their ionically dominant nature and the marginally enhanced tunnelling transmission in S0.5 when the moisture was being reduced.

3.4.3. Sensing stability under changing moisture content

It has been identified that the saturation degree of a water-saturated mortar is likely to settle at a range of 80 – 72.5% if exposed to the outside environment for a long term [116]. Based on the above analysis on the self-sensing performance of S0.5 and S1.2 at designated saturation degrees, it can be postulated that in Section 3.3, after a 3-day exposure to the environment, the sensors still had degree of water saturation above 30% whilst performing self-sensing tests at random saturation degrees, where the stress and electrical properties can be reasonability correlated (Fig. 10). Therefore, the sensing stability was defined as the variation of sensing sensitivity at a reduction of saturation degree from 80% to 50%, and the results were recorded in Table 2.

While using FCR_b as indicator, the sensitivity of S0.5 decreased by 24% but the sensitivity of S1.2 increased by 19%. Such a behaviour of S0.5 was in contrast to that reported in Wen and Chung's study where the sensing sensitivity of cement-based sensors containing 0.5 vol% of carbon fibres increased with the decreasing moisture content [59]. It is possible that such difference in behaviour results from the method for the control of moisture content. In Wen and Chung's study, the dried samples were re-submerged in water for only three days therefore the moisture might only enter the outer regions of the sample but not fully diffused into the bulk. Also, due to the ink-bottle effect, the water might not completely enter the pores when re-saturated from the dried state [117]. Therefore, it is possible that the condition of "wet state" in their study was close to the condition of the initial "dried state" with an ununiform moisture distribution, resulting in such different behaviour.

When characterized by FCR_b, under a decreasing saturation degree, the RGF of S0.5 had a continuous decrease (Fig. 15e) but the RGF of S1.2 had a continuous increase (Fig. 12b). This continuous change in sensitivity using macro-scale carbon fibres as conductive fillers was different from the fluctuational change in sensitivity using nano-scale conductive fillers in cement-based sensors, where the gauge factor initially increased from the lowest value at water saturation to the highest, then followed by a decrease [37,66]. Nano-scale conductive fillers, regardless of their aspect ratio, can be easily encapsulated by moisture due to comparable dimensions to capillary pores. Therefore, while changing the moisture content, the competitions between ionic conduction and electronic conduction can be more intense hence a fluctuational development of sensing sensitivity. In comparison, this study used macro-scale carbon fibres which can bridge across capillary pores hence a more consistent development of sensitivity under the changing moisture content in the pores.

While using FCX_c as an indicator, as the saturation degree decreased from 80% to 50%, the stress self-sensing sensitivities of both the sensors showed positive correlation to the saturation degree. The sensitivity of S0.5 had a decrease of 16% but the sensitivity of S1.2 had a greater

decrease of 30%. This can be ascribed to the moisture dependent nature of the piezopermittivity as described in Fig. 14.

4. Conclusions and recommendations

This study presents the stress self-sensing performance of cement-based sensors under the collective influence of moisture and fibre content. Interpretations on the piezopermittivity and piezoresistivity has been conducted based on the measured capacitive reactance and resistance by EIS. The mechanisms were described, and the self-sensing behaviour was discussed in comparison to the literature. The conclusions can be drawn as follows:

- Upon finishing drying, the porosity of plain mortar increased by 2.48% but the porosities of the cement-based sensors changed negligibly showing better resistance to microstructural damage of elevated temperature. The polarized light microscopy successfully revealed the location of the carbon fibres in the sensor's matrix, where the continuity of the electronic conduction pathway by the carbon fibres of sensor with 1.2 vol% of carbon fibre incorporation was better than that of sensor containing 0.5 vol% of carbon fibres.
- Regardless of the inclusion of the carbon fibres, the bulk arc of the impedance response can shrink in size under the increasing compressive stress indicating the increased conductance and capacitance. The bulk arc of the impedance response can extend in size under the decreasing moisture content, indicating the decreased system conductance and capacitance.
- After a 3-day exposure to the environment, the stress self-sensing performance of cement-based sensors was dominated by the fibre content. While increasing the fibre content, the sensing sensitivity increased but the sensing recoverability decreased. All samples exhibited sound sensing repeatability at stresses 0 – 6.375 MPa through three compressive loading and unloading cycles, regardless of the fibre content.
- While performing stress self-sensing at different saturation degrees, there existed differences in behaviour between sensors with 1.2 vol% of carbon fibres whose conduction of electricity is electrically dominant and sensor with 0.5 vol% of carbon fibres whose conduction of electricity is ionically dominant. The piezopermittivity is "moisture content-dominant" whilst the piezoresistivity is "fibre content-dominant". For an electronically dominant sensor, as the water saturation degree decreased, its sensitivity of piezoresistivity increased due to strong enhancement in tunnelling transmission but its sensitivity of piezopermittivity decreased due to loss of moisture. For an ionically dominant sensor, as the saturation degree decreased, its sensitivity of piezoresistivity decreased due to its marginal enhancement in tunnelling transmission and loss of moisture, and its sensitivity of piezopermittivity also decreased due to loss of moisture.
- While performing stress self-sensing at different saturation degrees, the pressure sensitive properties, piezoresistivity and piezopermittivity, behaved differently. For the electronically dominant sensor, the piezopermittivity is more sensitive than piezoresistivity at saturation degree of 80% but the piezoresistivity is more sensitive than piezopermittivity at lower saturation degrees of 50% and 30%. For the ionically dominant sensor, the piezoresistivity is more sensitive than piezopermittivity at the designated saturation degrees 80%, 50%, and 30%.
- It is recommended to use the sensor with 0.5 vol% of carbon fibres and the piezopermittivity as characterization indicator thanks to the lowest variation of sensitivity (i.e., 16%) while reducing the saturation degree from 80% to 50%. If the operation environment would cause large changes in the internal moisture content of the material, or if the variation in relative humidity of the operation environment is unknown, it is recommended to use the sensor with 1.2% of carbon fibre and the piezoresistivity as characterization indicator thanks to the consistent pressure sensitive response at all the saturation degrees 80%, 50%, and 30%.

For the first time, this study presents the difference in behaviour of piezoresistivity and piezopermittivity of carbon fibre reinforced cement-based sensors under the combined effects of moisture and fibre contents. This study has demonstrated that it is possible to use cement-based sensors with specified fibre contents under a humidity changing environment properly and efficiently without the need for extrinsic measures (i.e., water proofing techniques, extrinsic humidity sensor) as long as the sensing behaviour at various saturation degrees and the influence of the environment on the microstructure were strategically analysed prior to the deployment on site. The EIS technique has been shown to successfully differentiate the opposite behaviour of the piezopermittivity and piezoresistivity of sensor with 1.2 vol% of carbon fibres while changing the internal moisture, presenting a promising way for multi-parameter signal processing. It is recommended that if the sensors are facing multiple environmental effects at the same time (e.g., temperature/moisture variations, chloride/sulfuric ingression, freeze-thawing), EIS, with the virtue of non-invasive measurement, muti-parameter detection, and the flexibility of circuit modelling, can be combined with artificial intelligence techniques, for the differentiation and single-effect extraction of complex electrical and dielectric signal responses which were influenced by the complex environmental conditions and for the prediction of self-sensing behaviour of cement-based sensors under in-service conditions.

CRediT authorship contribution statement

Jiacheng Zhang: Conceptualization, Methodology, Investigation, Visualization, Writing – original draft, Writing – review & editing. **Andrew Heath:** Conceptualization, Methodology, Supervision, Writing – review & editing. **Richard J. Ball:** Conceptualization, Methodology, Supervision, Writing – review & editing. **Binling Chen:** Methodology, Writing – review & editing. **Linzhen Tan:** Methodology, Writing – review & editing. **Guisheng Li:** Supervision, Writing – review & editing. **Jingbang Pan:** Writing – review & editing. **Tugce Busra Su-Cadirci:** Investigation, Visualization. **Kevin Paine:** Conceptualization, Supervision, Funding acquisition, Writing – review & editing.

Declaration of Competing Interest

The authors declare that they have no known competing financial interests or personal relationships that could have appeared to influence the work reported in this paper.

Data Availability

Data will be made available on request.

Acknowledgements

The authors gratefully acknowledge the technical staff at the University of Bristol and within the Department of Architecture & Civil Engineering at the University of Bath for the technical support & assistance in this work. The Engineering and Physical Sciences Research Council (EPSRC) is thanked for funding the Resilient Materials for Life (RM4L) project (grant ID: EP/P02081X/1). The authors thank Professor Benny Suryanto at the Heriot-Watt University and Professor Antony Darby in the Department of Architecture & Civil Engineering at the University of Bath for their valuable suggestions on the paper.

References

[1] P.-W. Chen, D.D.L. Chung, Carbon fiber reinforced concrete for smart structures capable of non-destructive flaw detection, Smart Mater. Struct. 2 (1993) 22–30, https://doi.org/10.1088/0964-1726/2/1/004.

[2] P.-W. Chen, D.D.L. Chung, Improving the electrical conductivity of composites comprised of short conducting fibers in a nonconducting matrix: The addition of a nonconducting particulate filler, JEM 24 (1995) 47–51, https://doi.org/10.1007/BF02659726.

[3] D.D.L. Chung, Cement reinforced with short carbon fibers: a multifunctional material, Compos. Part B: Eng. 31 (2000) 511–526, https://doi.org/10.1016/S1359-8368(99)00071-2.

[4] D.D.L. Chung, Piezoresistive Cement-Based Materials for Strain Sensing, J. Intell. Mater. Syst. Struct. 13 (2002) 599–609, https://doi.org/10.1106/104538902031861.

[5] B. Han, J. Ou, Embedded piezoresistive cement-based stress/strain sensor, Sens. Actuators A: Phys. 138 (2007) 294–298, https://doi.org/10.1016/j.sna.2007.05.011.

[6] Baoguo Han Jinping Ou, Piezoresistive cement-based strain sensors and self-sensing concrete components, J. Intell. Mater. Syst. Struct. 20 (2009) 329–336, https://doi.org/10.1177/1045389×08094190.

[7] F. Azhari, N. Banthia, Cement-based sensors with carbon fibers and carbon nanotubes for piezoresistive sensing, Cem. Concr. Compos. 34 (2012) 866–873, https://doi.org/10.1016/j.cemconcomp.2012.04.007.

[8] B. Han, S. Ding, X. Yu, Intrinsic self-sensing concrete and structures: A review, Measurement 59 (2015) 110–128, https://doi.org/10.1016/j.measurement.2014.09.048.

[9] W. Dong, W. Li, Z. Tao, K. Wang, Piezoresistive properties of cement-based sensors: Review and perspective, Constr. Build. Mater. 203 (2019) 146–163, https://doi.org/10.1016/j.conbuildmat.2019.01.081.

[10] S. Ding, Y. Xiang, Y.-Q. Ni, V.K. Thakur, X. Wang, B. Han, J. Ou, In-situ synthesizing carbon nanotubes on cement to develop self-sensing cementitious composites for smart high-speed rail infrastructures, Nano Today 43 (2022) 101438, https://doi.org/10.1016/j.nantod.2022.101438.

[11] L. Wang, F. Aslani, Self-sensing performance of cementitious composites with functional fillers at macro, micro and nano scales, Constr. Build. Mater. 314 (2022) 125679, https://doi.org/10.1016/j.conbuildmat.2021.125679.

[12] B. Han, X. Yu, J. Ou, Self-sensing concrete in smart structures, Butterworth-Heinemann is an imprint of Elsevier, Amsterdam; Boston, 2014.

[13] X. Wang, S. Ding, Y.-Q. Ni, L. Zhang, S. Dong, B. Han, Intrinsic self-sensing concrete to energize infrastructure intelligence and resilience, J. Infrastruct. Intell. Resil. (2024) 100094, https://doi.org/10.1016/j.iintel.2024.100094.

[14] P.-W. Chen, D.D.L. Chung, Low-drying-shrinkage concrete containing carbon fibers, Compos. Part B: Eng. 27 (1996) 269–274, https://doi.org/10.1016/1359-8368(95)00020-8.

[15] P. Xie, P. Gu, J.J. Beaudoin, Electrical percolation phenomena in cement composites containing conductive fibres, J. Mater. Sci. 31 (1996) 4093–4097, https://doi.org/10.1007/BF00352673.

[16] S. Wen, D.D.L. Chung, Cement-based materials for stress sensing by dielectric measurement, Cem. Concr. Res. 32 (2002) 1429–1433, https://doi.org/10.1016/S0008-8846(02)00789-5.

[17] F. Reza, G.B. Batson, J.A. Yamamuro, J.S. Lee, Resistance Changes during Compression of Carbon Fiber Cement Composites, J. Mater. Civ. Eng. 15 (2003) 476–483, https://doi.org/10.1061/(ASCE)0899-1561(2003)15:5(476).

[18] S.-J. Lee, I. You, G. Zi, D.-Y. Yoo, Experimental Investigation of the Piezoresistive Properties of Cement Composites with Hybrid Carbon Fibers and Nanotubes, Sensors 17 (2017) 2516, https://doi.org/10.3390/s17112516.

[19] F.J. Baeza de los Santos, J.L. Vilaplana Abad, Ó. Galao Malo, P. Garcés Terradillos, Estudio de la sensibilidad a su propia deformación de escorias de alto horno activadas alcalinamente y reforzadas con fibra de carbono, Hormig. óN. Y. Acero 69 (2018) 243–250, https://doi.org/10.1016/j.hya.2017.04.008.

[20] Y. Hong, Z. Li, G. Qiao, J. Ou, W. Cheng, Pressure sensitivity of multiscale carbon-admixtures–enhanced cement-based composites, 184798041879352, Nanomater. Nanotechnol. 8 (2018), https://doi.org/10.1177/1847980418793529.

[21] D.D.L. Chung, Self-sensing concrete: from resistance-based sensing to capacitance-based sensing, Int. J. Smart Nano Mater. 12 (2021) 1–19, https://doi.org/10.1080/19475411.2020.1843560.

[22] L. Wang, F. Aslani, Mechanical properties, electrical resistivity and piezoresistivity of carbon fibre-based self-sensing cementitious composites, Ceram. Int. 47 (2021) 7864–7879, https://doi.org/10.1016/j.ceramint.2020.11.133.

[23] W. Pichór, M. Frąc, M. Radecka, Determination of percolation threshold in cement composites with expanded graphite by impedance spectroscopy, Cem. Concr. Compos. 125 (2022) 104328, https://doi.org/10.1016/j.cemconcomp.2021.104328.

[24] T. Sun, X. Wang, N. Maimaitituersun, S. Dong, L. Li, B. Han, Synergistic effects of steel fibers and steel wires on uniaxial tensile mechanical and self-sensing properties of UHPC, Constr. Build. Mater. 416 (2024) 134991, https://doi.org/10.1016/j.conbuildmat.2024.134991.

[25] R.M. Chacko, N. Banthia, A.A. Mufti, Carbon-fiber-reinforced cement-based sensors, Can. J. Civ. Eng. 34 (2007) 284–290, https://doi.org/10.1139/l06-092.

[26] B. Chen, J. Liu, Damage in carbon fiber-reinforced concrete, monitored by both electrical resistance measurement and acoustic emission analysis, Constr. Build. Mater. 22 (2008) 2196–2201, https://doi.org/10.1016/j.conbuildmat.2007.08.004.

[27] B. Han, X. Yu, E. Kwon, A self-sensing carbon nanotube/cement composite for traffic monitoring, Nanotechnology 20 (2009) 445501, https://doi.org/10.1088/0957-4484/20/44/445501.

[28] O. Galao, F.J. Baeza, E. Zornoza, P. Garcés, Strain and damage sensing properties on multifunctional cement composites with CNF admixture, Cem. Concr. Compos. 46 (2014) 90–98, https://doi.org/10.1016/j.cemconcomp.2013.11.009.

[29] G. Yildirim, G.H. Aras, Q.S. Banyhussan, M. Şahmaran, M. Lachemi, Estimating the self-healing capability of cementitious composites through non-destructive electrical-based monitoring, NDT E Int. 76 (2015) 26–37, https://doi.org/10.1016/j.ndteint.2015.08.005.

[30] Z. Tian, Y. Li, J. Zheng, S. Wang, A state-of-the-art on self-sensing concrete: Materials, fabrication and properties, Compos. Part B: Eng. 177 (2019) 107437, https://doi.org/10.1016/j.compositesb.2019.107437.

[31] S. Ding, X. Wang, L. Qiu, Y. Ni, X. Dong, Y. Cui, A. Ashour, B. Han, J. Ou, Self-Sensing Cementitious Composites with Hierarchical Carbon Fiber-Carbon Nanotube Composite Fillers for Crack Development Monitoring of a Maglev Girder, Small 19 (2023) 2206258, https://doi.org/10.1002/smll.202206258.

[32] P.L. Fuhr, D.R. Huston, Corrosion detection in reinforced concrete roadways and bridges via embedded fiber optic sensors, Smart Mater. Struct. 7 (1998) 217–228, https://doi.org/10.1088/0964-1726/7/2/009.

[33] B. Benmokrane, E. El-Salakawy, S. El-Gamal, S. Goulet, Construction and Testing of an Innovative Concrete Bridge Deck Totally Reinforced with Glass FRP Bars: Val-Alain Bridge on Highway 20 East, J. Bridge Eng. 12 (2007) 632–645, https://doi.org/10.1061/(ASCE)1084-0702(2007)12:5(632).

[34] H.M. Taha, R.J. Ball, A. Heath, K. Paine, Crack growth and closure in cementitious composites: Monitoring using piezoceramic sensors, Sens. Actuators A: Phys. 333 (2022) 113221, https://doi.org/10.1016/j.sna.2021.113221.

[35] N. Banthia, S. Djeridane, M. Pigeon, Electrical resistivity of carbon and steel micro-fiber reinforced cements, Cem. Concr. Res. 22 (1992) 804–814, https://doi.org/10.1016/0008-8846(92)90104-4.

[36] J. Cao, D.D.L. Chung, Electric polarization and depolarization in cement-based materials, studied by apparent electrical resistance measurement, Cem. Concr. Res. 34 (2004) 481–485, https://doi.org/10.1016/j.cemconres.2003.09.003.

[37] W. Dong, W. Li, N. Lu, F. Qu, K. Vessalas, D. Sheng, Piezoresistive behaviours of cement-based sensor with carbon black subjected to various temperature and water content, Compos. Part B: Eng. 178 (2019) 107488, https://doi.org/10.1016/j.compositesb.2019.107488.

[38] W.J. McCarter, S. Garvin, N. Bouzid, Impedance measurements on cement paste, J. Mater. Sci. Lett. 7 (1988) 1056–1057, https://doi.org/10.1007/BF00720825.

[39] W.J. McCarter, T.M. Chrisp, G. Starrs, J. Blewett, Characterization and monitoring of cement-based systems using intrinsic electrical property measurements, Cem. Concr. Res. 33 (2003) 197–206, https://doi.org/10.1016/S0008-8846(02)00824-4.

[40] W.J. McCarter, G. Starrs, T.M. Chrisp, The complex impedance response of fly-ash cements revisited, Cem. Concr. Res. 34 (2004) 1837–1843, https://doi.org/10.1016/j.cemconres.2004.01.013.

[41] W.J. McCarter, H.M. Taha, B. Suryanto, G. Starrs, Two-point concrete resistivity measurements: interfacial phenomena at the electrode–concrete contact zone, Meas. Sci. Technol. 26 (2015) 085007, https://doi.org/10.1088/0957-0233/26/8/085007.

[42] B.J. Christensen, T. Coverdale, R.A. Olson, S.J. Ford, E.J. Garboczi, H. M. Jennings, T.O. Mason, Impedance spectroscopy of hydrating cement-based materials: measurement, interpretation, and application, J. Am. Ceram. Soc. 77 (1994) 2789–2804, https://doi.org/10.1111/j.1151-2916.1994.tb04507.x.

[43] S. Ford, T. Mason, Combined Bulk and Interfacial Studies of the Cement/Steel System by Impedance Spectroscopy, in: N. Berke, E. Escalante, C. Nmai, D. Whiting (Eds.), Techniques to Assess the Corrosion Activity of Steel Reinforced Concrete Structures, ASTM International, 100 Barr Harbor Drive, PO Box C700, West Conshohocken, PA 19428-2959, 1996, https://doi.org/10.1520/STP16973S.

[44] G. Song, Equivalent circuit model for AC electrochemical impedance spectroscopy of concrete, Cem. Concr. Res. 30 (2000) 1723–1730, https://doi.org/10.1016/S0008-8846(00)00400-2.

[45] A. Peled, J.M. Torrents, T.O. Mason, S.P. Shah, Electrical Impedance Spectra to Monitor Damage during Tensile Loading of Cement Composites, MJ 98 (2001), https://doi.org/10.14359/10400.

[46] T.O. Mason, M.A. Campo, A.D. Hixson, L.Y. Woo, Impedance spectroscopy of fiber-reinforced cement composites, Cem. Concr. Compos. 24 (2002) 457–465, https://doi.org/10.1016/S0958-9465(01)00077-4.

[47] L.Y. Woo, S. Wansom, N. Ozyurt, B. Mu, S.P. Shah, T.O. Mason, Characterizing fiber dispersion in cement composites using AC-Impedance Spectroscopy, Cem. Concr. Compos. 27 (2005) 627–636, https://doi.org/10.1016/j.cemconcomp.2004.06.003.

[48] M. Cabeza, M. Keddam, X.R. Nóvoa, I. Sánchez, H. Takenouti, Impedance spectroscopy to characterize the pore structure during the hardening process of Portland cement paste, Electrochim. Acta 51 (2006) 1831–1841, https://doi.org/10.1016/j.electacta.2005.02.125.

[49] R.J. Ball, G.C. Allen, The measurement of water transport in porous materials using impedance spectroscopy, J. Phys. D: Appl. Phys. 43 (2010) 105503, https://doi.org/10.1088/0022-3727/43/10/105503.

[50] R.J. Ball, G.C. Allen, G. Starrs, W.J. McCarter, Impedance spectroscopy measurements to study physio-chemical processes in lime-based composites, Appl. Phys. A 105 (2011) 739–751, https://doi.org/10.1007/s00339-011-6509-7.

[51] R.J. Ball, G.C. Allen, M.A. Carter, M.A. Wilson, C. Ince, A. El-Turki, The application of electrical resistance measurements to water transport in

lime–masonry systems, Appl. Phys. A 106 (2012) 669–677, https://doi.org/10.1007/s00339-011-6653-0.
[52] G.L. Pesce, C.R. Bowen, J. Rocha, M. Sardo, G.C. Allen, P.J. Walker, G. Denuault, M. Serrapede, R.J. Ball, Monitoring hydration in lime-metakaolin composites using electrochemical impedance spectroscopy and nuclear magnetic resonance spectroscopy, Clay Min. 49 (2014) 341–358, https://doi.org/10.1180/claymin.2014.049.3.01.
[53] S.A. Grammatikos, R.J. Ball, M. Evernden, R.G. Jones, Impedance spectroscopy as a tool for moisture uptake monitoring in construction composites during service, Compos. Part A: Appl. Sci. Manuf. 105 (2018) 108–117, https://doi.org/10.1016/j.compositesa.2017.11.006.
[54] X. Wang, J. Zhang, R. Han, N. Han, F. Xing, Evaluation of damage and repair rate of self-healing microcapsule-based cementitious materials using electrochemical impedance spectroscopy, J. Clean. Prod. 235 (2019) 966–976, https://doi.org/10.1016/j.jclepro.2019.06.294.
[55] B. Díaz, B. Guitián, X.R. Nóvoa, C. Pérez, Analysis of the microstructure of carbon fibre reinforced cement pastes by impedance spectroscopy, Constr. Build. Mater. 243 (2020) 118207, https://doi.org/10.1016/j.conbuildmat.2020.118207.
[56] D. Saraireh, B. Suryanto, W.J. McCarter, S. Walls, The electro-mechanical tensile properties of an engineered cementitious composite, Adv. Cem. Res. 33 (2021) 478–495, https://doi.org/10.1680/jadcr.19.00119.
[57] J. Zhang, A. Heath, R.J. Ball, K. Paine, Effect of fibre loading on the microstructural, electrical, and mechanical properties of carbon fibre incorporated smart cement-based composites, Front. Mater. 9 (2022) 1055796, https://doi.org/10.3389/fmats.2022.1055796.
[58] Y. Wang, X. Zhao, POSITIVE AND NEGATIVE PRESSURE SENSITIVITIES OF CARBON FIBER-REINFORCEDCEMENT-MATRIX COMPOSITES AND THEIR MECHANISM, Acta Mater. Compos. Sin. 22 (2005) 40–46.
[59] S. Wen, D.D.L. Chung, Effect of Moisture on Piezoresistivity of Carbon Fiber-Reinforced Cement Paste, MJ 105 (2008) 274–280, https://doi.org/10.14359/19824.
[60] E. Teomete, The effect of temperature and moisture on electrical resistance, strain sensitivity and crack sensitivity of steel fiber reinforced smart cement composite, Smart Mater. Struct. 25 (2016) 075024, https://doi.org/10.1088/0964-1726/25/7/075024.
[61] E. Demircilioğlu, E. Teomete, E. Schlangen, F.J. Baeza, Temperature and moisture effects on electrical resistance and strain sensitivity of smart concrete, Constr. Build. Mater. 224 (2019) 420–427, https://doi.org/10.1016/j.conbuildmat.2019.07.091.
[62] B. Han, L. Zhang, J. Ou, Influence of water content on conductivity and piezoresistivity of cement-based material with both carbon fiber and carbon black, J. Wuhan. Univ. Technol. -Mat. Sci. Ed. 25 (2010) 147–151, https://doi.org/10.1007/s11595-010-1147-z.
[63] L. Zhang, S. Ding, B. Han, X. Yu, Y.-Q. Ni, Effect of water content on the piezoresistive property of smart cement-based materials with carbon nanotube/nanocarbon black composite filler, Compos. Part A: Appl. Sci. Manuf. 119 (2019) 8–20, https://doi.org/10.1016/j.compositesa.2019.01.010.
[64] M. Maier, The effect of moisture and reinforcement on the self-sensing properties of hybrid-fiber-reinforced concrete, Eng. Res. Express 2 (2020) 025026, https://doi.org/10.1088/2631-8695/ab90c7.
[65] B. del Moral, F.J. Baeza, R. Navarro, O. Galao, E. Zornoza, J. Vera, C. Farcas, P. Garcés, Temperature and humidity influence on the strain sensing performance of hybrid carbon nanotubes and graphite cement composites, Constr. Build. Mater. 284 (2021) 122786, https://doi.org/10.1016/j.conbuildmat.2021.122786.
[66] B. Han, X. Yu, J. Ou, Effect of water content on the piezoresistivity of MWNT/cement composites, J. Mater. Sci. 45 (2010) 3714–3719, https://doi.org/10.1007/s10853-010-4414-7.
[67] H. Wang, A. Zhang, L. Zhang, Q. Wang, X. Yang, X. Gao, F. Shi, Electrical and piezoresistive properties of carbon nanofiber cement mortar under different temperatures and water contents, Constr. Build. Mater. 265 (2020) 120740, https://doi.org/10.1016/j.conbuildmat.2020.120740.
[68] J.M. Cruz, I.C. Fita, L. Soriano, J. Payá, M.V. Borrachero, The use of electrical impedance spectroscopy for monitoring the hydration products of Portland cement mortars with high percentage of pozzolans, Cem. Concr. Res. 50 (2013) 51–61, https://doi.org/10.1016/j.cemconres.2013.03.019.
[69] B. Díaz, L. Freire, P. Merino, X.R. Nóvoa, M.C. Pérez, Impedance spectroscopy study of saturated mortar samples, Electrochim. Acta 53 (2007) 7549–7555, https://doi.org/10.1016/j.electacta.2007.10.042.
[70] S. Wen, D.D.L. Chung, Effect of admixtures on the dielectric constant of cement paste, Cem. Concr. Res. 31 (2001) 673–677, https://doi.org/10.1016/S0008-8846(01)00475-6.
[71] W.J. McCarter, G. Starrs, T.M. Chrisp, P.F.G. Banfill, Complex Impedance and Dielectric Dispersion in Carbon Fiber Reinforced Cement Matrices, J. Am. Ceram. Soc. 92 (2009) 1617–1620, https://doi.org/10.1111/j.1551-2916.2009.03057.x.
[72] J. Zhang, A. Heath, H.M.T. Abdalgadir, R.J. Ball, K. Paine, Electrical impedance behaviour of carbon fibre reinforced cement-based sensors at different moisture contents, Constr. Build. Mater. 353 (2022) 129049, https://doi.org/10.1016/j.conbuildmat.2022.129049.
[73] P.K. Sharma, N. Gupta, P.I. Dankov, Characterization of polydimethylsiloxane (PDMS) as a wearable antenna substrate using resonance and planar structure methods, AEU - Int. J. Electron. Commun. 127 (2020) 153455, https://doi.org/10.1016/j.aeue.2020.153455.
[74] G. Tai, D. Wei, M. Su, P. Li, L. Xie, J. Yang, Force-Sensitive Interface Engineering in Flexible Pressure Sensors: A Review, Sensors 22 (2022) 2652, https://doi.org/10.3390/s22072652.
[75] D.D.L. Chung, Sensing Materials: Self-Sensing Materials, in: Encyclopedia of Sensors and Biosensors, Elsevier, 2023, pp. 196–203, https://doi.org/10.1016/B978-0-12-822548-6.00004-2.
[76] S. Saga, Physical Sensors: Mechanical Sensors, in: Encyclopedia of Sensors and Biosensors, Elsevier, 2023, pp. 62–75, https://doi.org/10.1016/B978-0-12-822548-6.00031-5.
[77] D.D.L. Chung, X. Xi, Piezopermittivity for capacitance-based strain/stress sensing, Sens. Actuators A: Phys. 332 (2021) 113028, https://doi.org/10.1016/j.sna.2021.113028.
[78] X. Fu, E. Ma, D.D.L. Chung, W.A. Anderson, Self-monitoring in carbon fiber reinforced mortar by reactance measurement, Cem. Concr. Res. 27 (1997) 845–852, https://doi.org/10.1016/S0008-8846(97)83277-2.
[79] M. Ozturk, D.D.L. Chung, Capacitance-based stress self-sensing in asphalt without electrically conductive constituents, with relevance to smart pavements, Sens. Actuators A: Phys. 342 (2022) 113625, https://doi.org/10.1016/j.sna.2022.113625.
[80] Y. Wang, D.D.L. Chung, Capacitance-based nondestructive detection of aggregate proportion variation in a cement-based slab, Compos. Part B: Eng. 134 (2018) 18–27, https://doi.org/10.1016/j.compositesb.2017.09.015.
[81] D.D.L. Chung, Y. Wang, Capacitance-based stress self-sensing in cement paste without requiring any admixture, Cem. Concr. Compos. 94 (2018) 255–263, https://doi.org/10.1016/j.cemconcomp.2018.09.017.
[82] K. Shi, D.D.L. Chung, Piezoelectricity-based self-sensing of compressive and flexural stress in cement-based materials without admixture requirement and without poling, Smart Mater. Struct. 27 (2018) 105011, https://doi.org/10.1088/1361-665X/aad87f.
[83] Y. Hou, M. Sun, J. Chen, Electrical resistance and capacitance responses of smart ultra-high performance concrete with compressive strain by DC and AC measurements, Constr. Build. Mater. 327 (2022) 127007, https://doi.org/10.1016/j.conbuildmat.2022.127007.
[84] Z.S. Metaxa, Polycarboxylate based superplasticizers as dispersant agents for exfoliated graphene nanoplatelets reinforcing cement based materials, JESTR 8 (2015) 1–5, https://doi.org/10.25103/jestr.085.01.
[85] I. Papanikolaou, L. Ribeiro de Souza, C. Litina, A. Al-Tabbaa, Investigation of the dispersion of multi-layer graphene nanoplatelets in cement composites using different superplasticiser treatments, Constr. Build. Mater. 293 (2021) 123543, https://doi.org/10.1016/j.conbuildmat.2021.123543.
[86] H. Zhu, H. Zhou, H. Gou, Evaluation of carbon fiber dispersion in cement-based materials using mechanical properties, conductivity, mass variation coefficient, and microstructure, Constr. Build. Mater. 266 (2021) 120891, https://doi.org/10.1016/j.conbuildmat.2020.120891.
[87] H. Allam, F. Duplan, S. Amziane, Y. Burtschell, Assessment of manufacturing process efficiency in the dispersion of carbon fibers in smart concrete by measuring AC impedance, Cem. Concr. Compos. 127 (2022) 104394, https://doi.org/10.1016/j.cemconcomp.2021.104394.
[88] B. Han, L. Zhang, C. Zhang, Y. Wang, X. Yu, J. Ou, Reinforcement effect and mechanism of carbon fibers to mechanical and electrically conductive properties of cement-based materials, Constr. Build. Mater. 125 (2016) 479–489, https://doi.org/10.1016/j.conbuildmat.2016.08.063.
[89] W. Chuang, P. Lei, L. Bing-liang, G. Ni, Z. Li-ping, L. Ke-zhi, Influences of molding processes and different dispersants on the dispersion of chopped carbon fibers in cement matrix, Heliyon 4 (2018) e00868, https://doi.org/10.1016/j.heliyon.2018.e00868.
[90] H.F.W. Taylor, A method for predicting alkazi ion concentrations in cement pore solutions, Adv. Cem. Res. 1 (1987) 5–17, https://doi.org/10.1680/adcr.1987.1.1.5.
[91] D.C. Okpala, Pore structure of hardened cement paste and mortar, Int. J. Cem. Compos. Lightweight Concr. 11 (1989) 245–254, https://doi.org/10.1016/0262-5075(89)90105-X.
[92] Md.A.I. Laskar, R. Kumar, B. Bhattacharjee, Some aspects of evaluation of concrete through mercury intrusion porosimetry, Cem. Concr. Res. 27 (1997) 93–105, https://doi.org/10.1016/S0008-8846(96)00192-5.
[93] Z. Wu, H.S. Wong, N.R. Buenfeld, Transport properties of concrete after drying-wetting regimes to elucidate the effects of moisture content, hysteresis and microcracking, Cem. Concr. Res. 98 (2017) 136–154, https://doi.org/10.1016/j.cemconres.2017.04.006.
[94] B.W. Veal, P.M. Baldo, A.P. Paulikas, J.A. Eastman, Understanding Artifacts in Impedance Spectroscopy, J. Electrochem. Soc. 162 (2015) H47–H57, https://doi.org/10.1149/2.0791501jes.
[95] H.P. Schwan, C.D. Ferris, Four-Electrode Null Techniques for Impedance Measurement with High Resolution, Rev. Sci. Instrum. 39 (1968) 481–485, https://doi.org/10.1063/1.1683413.
[96] D.L. Johnson, P.N. Sen, Dependence of the conductivity of a porous medium on electrolyte conductivity, Phys. Rev. B 37 (1988) 3502–3510, https://doi.org/10.1103/PhysRevB.37.3502.
[97] B. Nettelblad, B. Ahlen, G.A. Niklasson, R.M. Holt, Approximate determination of surface conductivity in porous media, J. Phys. D: Appl. Phys. 28 (1995) 2037–2045, https://doi.org/10.1088/0022-3727/28/10/007.
[98] S. Grimnes, Ø.G. Martinsen. Bioimpedance and bioelectricity basics, Third edition, Elsevier/Academic Press, Amsterdam Boston Heidelberg London, 2015.
[99] B. Suryanto, W.J. McCarter, G. Starrs, G.V. Ludford-Jones, Electrochemical immittance spectroscopy applied to a hybrid PVA/steel fiber engineered cementitious composite, Mater. Des. 105 (2016) 179–189, https://doi.org/10.1016/j.matdes.2016.05.037.

[100] W.J. McCarter, B. Suryanto, H.T. Abdalgadir, G. Starrs, J. Kim, Features of Immittance Spectra as Performance Indicators for Cement-Based Concretes, Adv. Cem. Res. (2022) 1–38, https://doi.org/10.1680/jadcr.22.00023.
[101] W.J. McCarter, R. Brousseau, The A.C. response of hardened cement paste, Cem. Concr. Res. 20 (1990) 891–900, https://doi.org/10.1016/0008-8846(90)90051-X.
[102] J. Holly, D. Hampton, M.D.A. Thomas, Modelling relationships between permeability and cement paste pore microstructures, Cem. Concr. Res. 23 (1993) 1317–1330, https://doi.org/10.1016/0008-8846(93)90069-L.
[103] A. Korpa, R. Trettin, The influence of different drying methods on cement paste microstructures as reflected by gas adsorption: Comparison between freeze-drying (F-drying), D-drying, P-drying and oven-drying methods, Cem. Concr. Res. 36 (2006) 634–649, https://doi.org/10.1016/j.cemconres.2005.11.021.
[104] C. Gallé, Effect of drying on cement-based materials pore structure as identified by mercury intrusion porosimetry: A comparative study between oven-, vacuum-, and freeze-drying, Cem. Concr. Res. 31 (2001) 1467–1477, https://doi.org/10.1016/S0008-8846(01)00594-4.
[105] K.K. Aligizaki, Pore Structure of Cement-Based Materials: Testing, Interpretation and Requirements, 0 ed, CRC Press, 2005, https://doi.org/10.1201/9781482271959.
[106] L. Zhang, F.P. Glasser, Critical examination of drying damage to cement pastes, Adv. Cem. Res. 12 (2000) 79–88, https://doi.org/10.1680/adcr.2000.12.2.79.
[107] M. Atiyeh, E. Aydin, Carbon-Fiber Enriched Cement-Based Composites for Better Sustainability, Materials 13 (2020) 1899, https://doi.org/10.3390/ma13081899.
[108] W. Li, F. Qu, W. Dong, G. Mishra, S.P. Shah, A comprehensive review on self-sensing graphene/cementitious composites: a pathway toward next-generation smart concrete, Constr. Build. Mater. 331 (2022) 127284, https://doi.org/10.1016/j.conbuildmat.2022.127284.
[109] S. Wen, D.D.L. Chung, Model of piezoresistivity in carbon fiber cement, Cem. Concr. Res. 36 (2006) 1879–1885, https://doi.org/10.1016/j.cemconres.2006.03.029.
[110] J. Xu, W. Zhong, W. Yao, Modeling of conductivity in carbon fiber-reinforced cement-based composite, J. Mater. Sci. 45 (2010) 3538–3546, https://doi.org/10.1007/s10853-010-4396-5.
[111] J. Xu, W. Yao, R. Wang, Nonlinear conduction in carbon fiber reinforced cement mortar, Cem. Concr. Compos. 33 (2011) 444–448, https://doi.org/10.1016/j.cemconcomp.2010.10.007.
[112] S. Ding, S. Dong, A. Ashour, B. Han, Development of sensing concrete: Principles, properties and its applications, J. Appl. Phys. 126 (2019) 241101, https://doi.org/10.1063/1.5128242.
[113] M. Moukwa, P.-C. Aïtcin, The effect of drying on cement pastes pore structure as determined by mercury porosimetry, Cem. Concr. Res. 18 (1988) 745–752, https://doi.org/10.1016/0008-8846(88)90098-1.
[114] M. Sun, Z. Li, Q. Mao, D. Shen, Study on the Hole Conduction Phenomenon in Carbon Fiber-Reinforced Concrete, Cem. Concr. Res. 28 (1998) 549–554, https://doi.org/10.1016/S0008-8846(98)00011-8.
[115] E. Barsoukov, J.R. Macdonald (Eds.), Impedance spectroscopy: theory, experiment, and applications, 2nd ed, Wiley-Interscience, Hoboken, N.J, 2005.
[116] J. Bao, S. Li, P. Zhang, S. Xue, Y. Cui, T. Zhao, Influence of exposure environments and moisture content on water repellency of surface impregnation of cement-based materials, J. Mater. Res. Technol. 9 (2020) 12115–12125, https://doi.org/10.1016/j.jmrt.2020.08.046.
[117] F. Rajabipour, J. Weiss, Electrical conductivity of drying cement paste, Mater. Struct. 40 (2007) 1143–1160, https://doi.org/10.1617/s11527-006-9211-z.